Cathode Materials and Chemistries for Magnesium Batteries: Challenges and Opportunities

Zhenyou Li,* Joachim Häcker, Maximilian Fichtner, and Zhirong Zhao-Karger*

Rechargeable magnesium batteries hold promise for providing high energy density, material sustainability, and safety features, attracting increasing research interest as post-lithium batteries. With the progressive development of Mg electrolytes with enhanced (electro-)chemical stability, tremendous efforts have been devoted to the exploration of high-energy cathode materials. In this review, recent findings related to Mg cathode chemistry are summarized, focusing on the strategies that promote Mg^{2+} diffusion by targeting its interaction with the cathode hosts. The critical role of the cathode–electrolyte interfaces is elaborated, which remains largely unexplored in Mg systems. The approaches to optimization of cathode–electrolyte combinations to unlock the kinetic limitations of Mg^{2+} diffusion, enabling fast electrochemical processes of the cathodes, are highlighted. Furthermore, representative conversion chemistries and coordination chemistries that bypass bulk Mg^{2+} diffusion are discussed, with particular attention given to their key challenges and prospects. Finally, the hybrid systems that combine the fast kinetics of the monovalent cathode chemistries and high-capacity Mg anodes are revisited, calling for further practical evaluation of this promising strategy. All in all, the aim is to provide fundamental insights into the cathode chemistry, which promotes the material development and interfacial regulations toward practical high-performance Mg batteries.

1. Introduction

The urgent demand to significantly reduce the carbon footprint stimulates the development of electrochemical energy storage (EES) technologies, which provide the most suitable output characteristics for the application of renewable energies.[1] Lithium-ion batteries (LIBs) represent the state-of-the-art EES technology by exhibiting currently the most balanced application metrics.[2] Consequently, the production already increases to gigafactory level and the market reaches out toward e-mobility, smart grids, and even electric aviation.[3] However, the long-term supply of raw materials on a tremendous scale may be restricted by the low abundance (22 ppm in the Earth's crust) and the current poor recycling rate (<1%)[4] of lithium. Moreover, further pushing the energy density by applying Li metal anode faces intrinsic challenges associated with easy dendrite formation, which raises critical safety concern.[5]

Tackling these challenges requires transformative innovations by developing performance-wise competitive chemistries that are less dependent on Li, preferably based on earth-abundant elements.[6] A more sustainable system can therefore be achieved by applying multivalent metals with a larger atom fraction in the earth crust, for example, magnesium (Mg) ion, as charge carrier.[7] Compared to other storage ions, Mg^{2+} can be reduced to their metallic form with a more homogenous morphology,[8] exhibiting a dendrite-free deposition at practical current densities.[9] The unique physicochemical properties enable safer implementation of a metal anode, which provides theoretically high volumetric capacity,[10] offering an alternative pathway to achieve high energy density systems.[11]

High-performance Mg batteries rely on the efficient and reversible shuttling of Mg^{2+} between the cathode and the anode. However, the bivalent nature of the charge carriers renders a significant polarizing effect, generating strong interactions with polar species or moieties.[12] As a result, ion mobility in both non-aqueous solutions (electrolytes) and solids (cathode materials) is

Z. Li, M. Fichtner, Z. Zhao-Karger
Helmholtz Institute Ulm (HIU) Electrochemical Energy Storage
Helmholtzstraße 11, D-89081 Ulm, Germany
E-mail: zhenyou.li@kit.edu; zhirong.zhao-karger@kit.edu

Z. Li
Qingdao Institute of Bioenergy and Bioprocess Technology
Chinese Academy of Sciences
No. 189 Songling Road, Laoshan District, Qingdao, Shandong 266101, China
J. Häcker
Institute of Engineering Thermodynamics
Department of Electrochemical Energy Technology
German Aerospace Center (DLR)
Pfaffenwaldring 38–40, 70569 Stuttgart, Germany
M. Fichtner, Z. Zhao-Karger
Institute of Nanotechnology (INT)
Karlsruhe Institute of Technology (KIT)
P.O. Box 3640, D-76021 Karlsruhe, Germany

ADVANCED
SCIENCE NEWS

www.advancedsciencenews.com

**ADVANCED
ENERGY
MATERIALS**

www.advenergymat.de

limited.[13] The diffusivity of Mg^{2+} in solution environment can be enhanced by promoting the dissociation of electrolyte applying either strong chelating solvent (such as ethers) or auxiliary anions with high electronegativity (such as chloride ions).[14] Based on these findings, various types of Mg electrolytes[15–17] were developed and further optimized with improved chemical and electrochemical compatibility.

Compared to a solution environment, Mg^{2+} diffusion in solid hosts is even more challenging: on the one hand there is no assisting agent available in the solid environment to shield the high charge density; on the other hand, ion hopping in rigid crystal structures within relatively narrow spacing suffers from even stronger interactions.[13] Despite progressive findings on the screening and design of functioning cathode materials, the lack of host structures that enables sufficient cation mobility without compromising capacity or voltage remains a bottleneck for the development of Mg batteries.[18,19]

Notably, recent findings indicate that the cathode chemistry of Mg systems might involve multiple rate-determining processes.[20] In addition to solid diffusion, mass transfer at the cathode–electrolyte interface needs to overcome high activation energy associated with desolvation/dissociation.[21,22] The interfacial issue limits the magnesiation of cathode hosts to a low degree, but also generates overpotentials that reduce the storage efficiency. In fact, without well-established model systems, investigation of the sluggish reaction kinetics at the cathode side requires to consider all the ir-/reversible processes within the whole charge loop.[23,24]

In this review, we put the solid diffusion of Mg^{2+} in a broader context and summarize established strategies toward enabling viable cathode chemistries for Mg batteries. Tackling the intrinsic issue of sluggish diffusion kinetics, approaches applied to weaken the Mg^{2+}–cathode interaction is first described in Section 2. A focus will be on the development of insertion compounds with flexible electronic configurations and favorable crystallographic structures. Efforts made to reduce the charge density of Mg^{2+} are also elaborated. Rather than isolating the solid diffusion process, it is attempted to emphasize the importance of related crossover issues at the cathode side. This will be addressed in Section 3, by highlighting how cathode interfacial properties can be tuned to promote subsequent Mg diffusion. Alternatively, we showcase systems that circumvent polarizing divalent ion diffusion in Section 4, covering conversion cathodes and hybrid batteries. Finally, we bring our perspective for better understanding of the reactions and transport processes at the cathode side toward designing practical Mg batteries.

2. Weaken the Mg^{2+}–Cathode Interaction

Mg-ions suffer from sluggish mobility in solids due to their strong interaction with polar groups of the host lattice, which build up the diffusion pathways. Therefore, a comprehensive understanding of crystallographic structure as well as electronic structure of the insertion compounds is essential to screen favorable geometries for Mg-ion migration. Meanwhile, the gained knowledge allows fine tuning of the local structure by crystal engineering strategies, which further reduce the migration energy barrier. In addition, the ion–dipole interactions can also be alleviated if the double charge of the Mg-ion is properly shielded.

In this section, strategies based on the structural effect on Mg-ion diffusion and novel Mg-based insertion chemistries are discussed.

2.1. Crystal Structure Design and Engineering

The redox potential of cathode materials determines the output voltage of Mg metal-based full cells. A high-voltage cathode is therefore of practical importance, as the electrochemical potential of Mg is 0.7 V higher than that of Li and 0.5 V higher than the de-/lithiation of graphite,[25] leading to a considerable decrease of the cell voltage. Since Mg^{2+} (0.72 Å) has a similar ionic radius as Li$^+$ (0.76 Å),[26] a simple thought would be to investigate Mg storage capability in well-established high-voltage cathode materials for LIBs. However, significant degradation of storage performance was evident in a broad range of candidates when shifting from monovalent to Mg systems.[13,18] This implies different storage properties and diffusion mechanisms of Mg^{2+} compared to the monovalent ions. Therefore, developing lattice frameworks for decent Mg mobility needs to consider the preferential coordination environment of Mg^{2+} and its motion behavior in solids.

2.1.1. Transition Metal (TM) Oxides: MnO$_2$ and V$_2$O$_5$

Among the reported materials, manganese dioxide (MnO$_2$) and vanadium pentoxide (V$_2$O$_5$) seemed to arouse the most interest due to their plentiful polymorphs and various oxidation states of the TMs, which offer tunable electrochemical properties.[27,28] The polymorphism of MnO$_2$ originates from the six-coordination of Mn by O, which can be either edge-shared or corner-shared between the neighboring octahedrals with different stacking orders.[29] The first studied polymorph was α-MnO$_2$ (Hollandite) with 1D diffusion channels as large as $\approx$5 Å in size, which should provide enough space for the transport of Mg^{2+}.[30] Reversible de-/magnesiation of α-MnO$_2$ got both experimental and theoretical support, but was limited to a low Mg content (Mg/Mn < 0.26).[31,32] Deep magnesiation led to collapse of the diffusion tunnels[30] and amorphization of the material,[33] contributing to a sharp increase of the migration barrier.

To get more insights into the de-/magnesiation processes in MnO$_2$, a systematic electrochemical evaluation was carried out for different MnO$_2$ polymorphs with controlled physical parameters.[27] The result suggested that the Mg storage performance was almost independent on the crystal structure (**Figure 1**a), having rather a strong correlation with the surface area of the samples (Figure 1b). Further mechanistic analysis revealed a conversion pathway for MnO$_2$ during the insertion/extraction of Mg^{2+}.[33] According to density functional theory (DFT) studies, Mg^{2+} has strong affinity to O^{2-}, which drives the reaction toward the formation of MgO and MnO instead of an intercalated Mg$_x$MnO$_2$ compound (Figure 1c).[31] These findings clearly indicate the unique features of Mg-based chemistry, when compared with Li. Nevertheless, it should be mentioned that the conversion mechanism of MnO$_2$ is still controversial. On the one hand, the DFT study considered kinetical hindrance of the phase transition to a spinel structure.[31] On the other hand, the incompatibility between TM oxide and Cl-based electrolyte needs to be
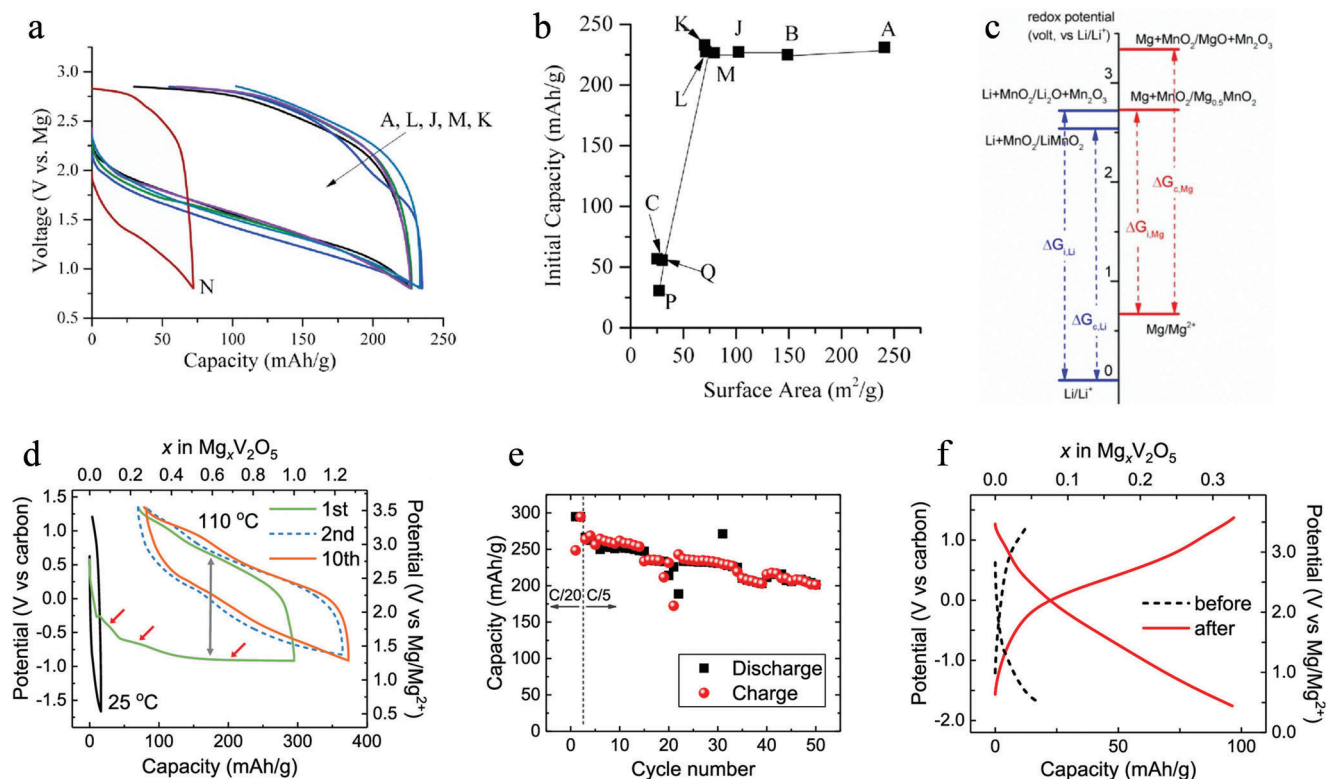
ADVANCED
SCIENCE NEWS

www.advancedsciencenews.com

ADVANCED
ENERGY
MATERIALS

www.advenergymat.de

Figure 1. a) Mg storage in various MnO$_2$ polymorphs. b) Relationship between the surface area of MnO$_2$ and their initial magnesiation capacity. The capital letters represent different MnO$_2$ structures. Reproduced with permission.[27] Copyright 2015, Elsevier. c) Thermodynamics of Li and Mg storage in MnO$_2$. Reproduced with permission.[31] Copyright 2015, American Chemical Society. d) Voltage profiles of Mg storage in α-V$_2$O$_5$ at different temperatures. e) Cycling performance of α-V$_2$O$_5$ at 110 °C. f) De-/magnesiation profiles of α-V$_2$O$_5$ at room temperature before and after activation at 110 °C. Reproduced with permission.[34] Copyright 2019, American Chemical Society.

clarified.[17] In fact, a very recent report demonstrated an impressive reversible Mg storage in layered Mg$_{0.15}$MnO$_2$ by manipulating the solvation structure of Mg^{2+} in the electrolyte, pointing out interfacial issues in addition to the sluggish diffusion.[20]

V$_2$O$_5$ is another high-voltage cathode material which has attracted attention. With a typical layered structure, α-V$_2$O$_5$ provides theoretically high specific energy of 737 Wh kg^{-1} at material level based on the storage of one Mg per V$_2$O$_5$ unit at a voltage of ≈2.5 V.[28] But unlike MnO$_6$ octahedrals, VO$_5$ pyramids are the building blocks that form the diffusion channels with Mg^{2+} stored in an eight-coordinated site. In the material, migration of Mg^{2+} has to undergo a drastic change of the coordination environment through a three-coordinated site, requiring a high activation energy of ≈1000 meV. Compared to α-V$_2$O$_5$, δ-V$_2$O$_5$ offers a kinetically more favorable diffusion pathway for Mg^{2+} by activating a multistep migration with a smaller coordination change.[28] However, despite of a more reasonable, but still high migration energy of 600−760 meV, experimental validation of δ-Mg$_x$V$_2$O$_5$ is still pending. In fact, δ-MgV$_2$O$_5$ phase (isostructural with δ-LiV$_2$O$_5$)[35] can be obtained only by chemical magnesiation of α-V$_2$O$_5$.[36] Achieving such high Mg^{2+} content by electrochemical approach requires a two-electron redox, which is challenging.[37] Practical Mg^{2+} insertion levels in various V$_2$O$_5$ polymorphs from dry organic electrolyte are much smaller (max. Mg$_{0.3}$V$_2$O$_5$).[38]

A recent work demonstrated that high temperature (110 °C) enables α-V$_2$O$_5$ to reversibly uptake and release one Mg^{2+}, amounting to a capacity of 280 mAh g^{-1}, which is almost the theoretical value (Figure 1d,e).[34] A significantly improved capacity of 100 mAh g^{-1} can be retained after the high temperature activation when the cell is cycled at room temperature (Figure 1f). However, structural characterizations indicate a different phase transition than previously predicted,[36] neither ϵ-Mg$_{0.5}$V$_2$O$_5$ nor δ-MgV$_2$O$_5$. Determination of the magnesiated compounds is highly demanded to fully understand the redox processes that contribute to the excellent performance. It should also be noted that the study utilized an ionic liquid electrolyte, which might circumvent desolvation of Mg^{2+}.[39] Such interfacial phenomena were also investigated in other studies[40] and will be discussed in the following section.

2.1.2. Structural Design for Favorable Diffusion Pathways

In typical TM compounds, TM cations are surrounded by anions, which build up the diffusion pathways for the intercalants. Shifting from oxide framework down to sulfides or even selenides provides an easier polarizable diffusion environment, thereby leading to a smaller migration barrier. Taking layered vanadium dichalcogenides as an example, Mg^{2+} occupies a thermodynamically stable octahedral site and has to pass through an
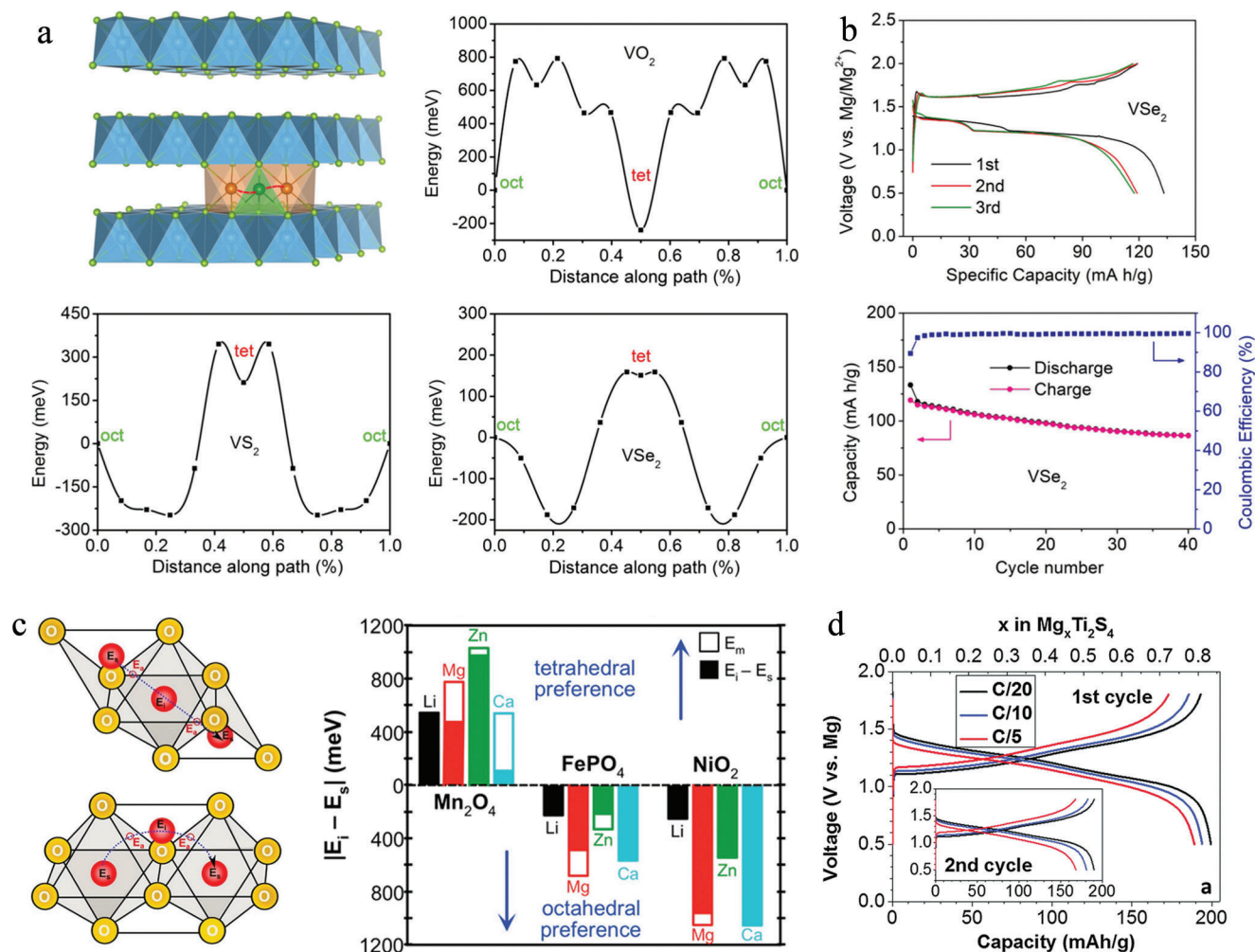
Figure 2. a) Diffusion energy profile of Mg^{2+} in vanadium dichalcogenides. b) Battery performance of VSe_2 against Mg. Reproduced with permission.[41] Copyright 2019, American Chemical Society. c) Site preference and hopping mechanism in typical insertion cathodes. Reproduced with permission.[42] Copyright 2015, American Chemical Society. d) Voltage profiles of Mg storage in spinel Ti_2S_4. Reproduced with permission.[45] Copyright 2016, The Royal Society of Chemistry.

intermediate tetrahedral site to reach the next equivalent stable site.[41] Even considering a dilute Mg concentration, the maximum barrier along the diffusion path for VO_2 is as high as 1032 meV, which is far beyond the estimated energy threshold required for moderate kinetics (525–650 meV). The value in VS_2 (593 meV) becomes more attractive, which further decreases to 346 meV in VSe_2 (**Figure 2**a).[42] The energetic advantage of VSe_2 gives rise to distinct intercalation plateaus in the voltage profile with high reversibility (Figure 2b).[43] Other selenide compounds also exhibit promising rate capability and deliver high volumetric energy density, which can be even higher than that of $LiCoO_2$.[18,44] However, their practical application is restricted by the low output voltage ($\approx$1 V) and the environmental impact of Se.

To design favorable diffusion pathways, site preference of the intercalant is another key factor. Mg^{2+} prefers a six-coordination while Li^+ favors a four-coordination in the host structure.[46] In both olivine and layered structure, the most successful cathodes for Li storage, the stable insertion site is six-coordinated. Con-sidering a minimum energy path, the intercalant needs to hop through a four-coordinated tetrahedral site in order to migrate between the adjacent octahedral sites.[41] As the tetrahedral site is favorable for Li^+, its oct–tet–oct hopping gets facilitated, resulting in a low migration energy. On the other hand, migration of Mg^{2+} from its preferential coordination site to an unfavorable site leads to a high energy barrier that impedes Mg^{2+} mobility at room temperature.[47] Following this guideline, materials that allow Mg^{2+} migration through an octahedral metastable site could be promising candidates.

It was found that the spinel structure meets the abovementioned requirement, by providing stable tetrahedral sites for Mg^{2+} storage, which is bridged by face-shared octahedral intermediate site (Figure 2c).[48] DFT calculations indicate that the energy barrier for Mg^{2+} diffusion in various spinel oxides (Mn_2O_4, Co_2O_4, Cr_2O_4, and Ni_2O_4) falls into the range of 650–850 meV, which is smaller than that of layered oxides and already close to the threshold value for moderate ion mobility.[49] Theoretically, Mg insertion in spinel oxides could take place at a considerably
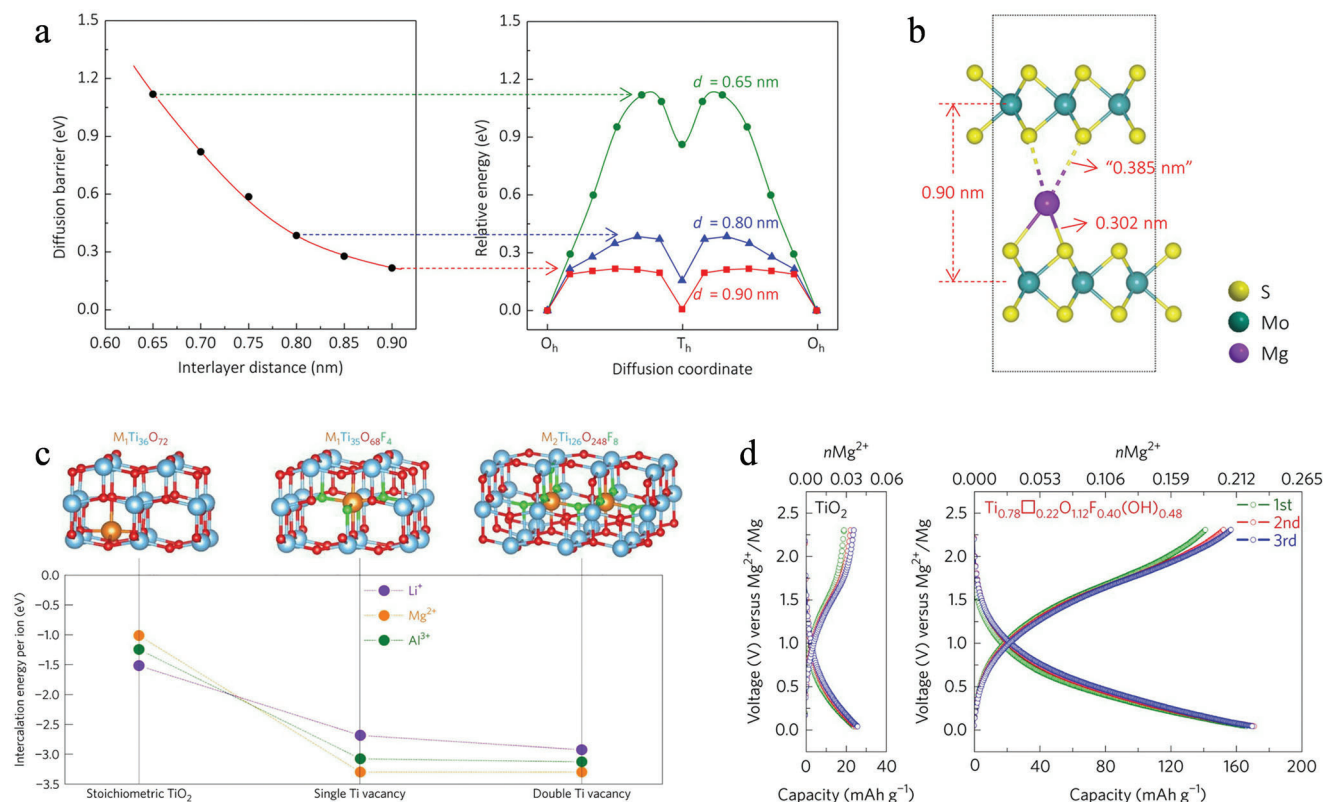
**ADVANCED
SCIENCE NEWS**

www.advancedsciencenews.com

**ADVANCED
ENERGY
MATERIALS**

www.advenergymat.de

Figure 3. a) Diffusion barrier for Mg^{2+} in layered MoS_2 with different d-spacing. b) Asymmetric Mg distance in MoS_2 molecular layers. Reproduced with permission.[58] Copyright 2015, American Chemical Society. c) A comparison of Li^+, Mg^{2+}, and Al^{3+} intercalation in defect-free TiO_2 and vacancy-doped TiO_2, respectively. d) Voltage profiles of defect-free TiO_2 and vacancy-doped TiO_2 upon de-/magnesiation. Reproduced with permission.[60] Copyright 2017, Springer Nature.

high voltage close to 3.0 V versus Mg, delivering a capacity of >200 mAh g^{-1}.[50] However, such promising performance seems to be only possible at elevated temperature >150 °C in experiments.[51] In addition to the high migration barrier, cation disorder with the formation of a rocksalt structure results in Mg^{2+} being stored at a stable octahedral site rather than the desired tetrahedral site, which inhibits further Mg mobility.[52]

As a compromised approach, thiospinels with "softer" S anions were proposed for Mg storage.[53] Compared to spinel oxides, thiospinels exhibited reasonably low diffusion energy barriers even down to 515 meV (in Mn_2S_4) for Mg^{2+}, which is adequate for moderate charging rate in a battery.[53] Experimental demonstration of reversible Mg insertion in thiospinel was first carried out in Ti_2S_4.[45] As shown in Figure 2d, magnesiation of Ti_2S_4 spinel exhibited a solid solution behavior with a voltage slope between 1.5 and 1.0 V, delivering a capacity of ≈200 mAh g^{-1} at 60 °C, which outperforms the layered TiS_2.[54,55] Multimodal characterization revealed only 10% volume expansion upon insertion and a Mg^{2+} diffusivity of 5×10^{-10} cm^2 s^{-1},[56] contributing to a fairly good rate capability as well as cycling stability.[45] Room temperature operation of the spinel Ti_2S_4-based Mg cell was also feasible, but limited to a rather low C-rate (C/50). Interestingly, it was found that Mg^{2+} first occupies the octahedral 16c sites in Ti_2S_4 spinel instead of the tetrahedral 8a sites, as would be expected in a normal spinel.[57] The tetrahedral occupation occurs only at a high Mg^{2+} content exceeding $Mg_{0.6}Ti_2S_4$ and might block the mi-

gration of Mg^{2+} resides in the adjacent octahedral sites. This finding might hint at possible high energy barriers related to insertion into the stable tetrahedral site, which provides unfavorable coordination for Mg^{2+}. Full understanding of the abnormal occupancy requires further investigation of other thiospinels such as Mn_2S_4 and Cr_2S_4, however.

2.1.3. Engineering Mg^{2+} Diffusion Channels

Crystal engineering approaches herein refer to efforts devoted to modifying the known structures for enhanced Mg storage. An effective way to mitigate trapping effect of the host lattice is therefore to increase the physical distance between Mg^{2+} and the host lattice by enlarging the diffusion channels. This strategy was validated in molybdenum disulfide, which has a layered structure.[58] The weak van der Waals forces between molecular layers renders a widely tunable interlayer distance.[59] Theoretical investigation of Mg^{2+} in MoS_2 shown in **Figure 3**a, indicated a significant decrease of the diffusion barrier with expanded interlayer distance. A comparable diffusivity to that of Li^+ in original MoS_2 structure ($d = 0.62$ nm) can be achieved when increasing the value to 0.772 nm (25% increase).[58] Further increasing the d-spacing does not facilitate Mg mobility anymore, but rather leads to an asymmetric Mg distance between the layers, where Mg is only effectively bonding to one MoS_2 layer

ADVANCED
SCIENCE NEWS

www.advancedsciencenews.com

ADVANCED
ENERGY
MATERIALS

www.advenergymat.de

(see Figure 3b). This resembles a surface reaction with the coordination number of Mg^{2+} reduced from six to three. Such storage mechanism was further revealed in other expanded 2D transition metal sulfides (TMSs) such as TiS_2 and was found beneficial for accommodating larger Mg-based cations.[22]

In principle, this approach can be extended to any structures that are constructed by weak van der Waals interaction, including 1D vanadium tetrasulfide,[61] 2D TM oxides,[62] and other layered materials.[63] Even for spinel structures, a 5% volume expansion is enough to bring down the migration barrier by ≈200 meV, amounting to approximately four order of magnitude improvement in diffusion.[55] However, it should be noted that expansion of the structure by self-adjustment (e.g., disordering) is limited to 10%.[58] Stabilizing pillars (organics or water molecules) are normally applied to get a desired extend of enlargement. However, the pillars also bring negative side effects by, for example, occupying the Mg^{2+} sites, lowering the electronic conductivity of the cathode, or triggering proton shuttling.[62,64] In addition, enlarging the distance between Mg^{2+} and the host lattice is penalized by reduced voltage as well as low bulk density, leading to a lower energy density.

Other than engineering the "natural" diffusion channels resulted from ordered atomic packing, creating new voids in known structures could also be a feasible option. The idea is to partially circumvent Mg migration through the original high-barrier diffusion pathways, by building additional tunnels with low activation energy. Introducing cationic vacancies in anatase TiO_2 unlocked its electrochemical activity upon reversible de-/magnesiation at room temperature (Figure 3c,d).[60] Compared to the defect-free TiO_2 (25 mAh g^{-1}), vacancy-doped TiO_2 delivered a significant improved capacity of 165 mAh g^{-1} with excellent rate capability and cycling stability. At a high vacancy level (22%), a vacancy-mediated diffusion mechanism was revealed, indicating its kinetic advantages. Similar observations were made on MoO_3, where F^- substitution generated Mo vacancies that offered additional basal plane diffusion pathways for fast Mg^{2+} migration.[65]

Due to the high tendency of cation disordering with Mg,[49] cation vacancies in TM compounds may also provide a thermodynamically favorable driving force for Mg^{2+} insertion. Ideally, highly concentrated vacancies with homogeneous distribution among the cathode structure could build a percolating network, serving as Mg diffusion highways.[66] Note that a high vacancy level means an off-stoichiometry of the redox active TM to a large extent, reducing the accessible capacity. On the other hand, anionic vacancies in TiO_2 were found feasible as well to promote Mg diffusion,[67] probably by providing a less-oxygen environment. Overall, defect chemistry opens a new avenue for efficient Mg storage, calling for further exploration in high-voltage cathodes.[51]

2.2. Compounds with Delocalized Electronic Structure

The bivalency of Mg^{2+} not only leads to kinetic limitations impeded by strong electrostatic interaction with the host lattice, but also alters the thermodynamic preference by forming stable conversion products.[31] Hosting a double charged Mg^{2+} would have greater impact on the local structure than a monovalent Li^+ occupancy. In addition to the lattice environment, local charge balancing and polarizability of the host structure are equally important.[68] This is particularly the case for the TM compounds. Typical TM ions can only afford one-electron redox and their coordination is sensitive to oxidation states, inducing local structural deformation upon magnesiation.[13,69] To have smaller influence on local electronic structures, strategies that allow proper charge allocation among the lattice are desired. From thermodynamic point of view, this would require multiple redox centers to provide their valence bands at a similar energy level that renders the compounds with delocalized electronic structure.[43]

2.2.1. Cluster Compounds

In 2000, Aurbach et al. demonstrated the first Mg cell prototype with excellent rate capability and remarkable cycle life.[7] This breakthrough was possible by applying Chevrel phase Mo_6S_8 cathode, which exhibits high Mg^{2+} mobility at room temperature. The high ionic conductivity of the Chevrel phase originates from its unique cluster structure constructed by Mo_6S_8 blocks, where a Mo_6 octahedron is caged by an S_8 cube.[70] Due to the metallic Mo–Mo bonding inducing delocalized electronic structure, six Mo in the octahedron share the double charge (Mg^{2+} at outer ring site as shown in **Figure 4**a), resulting in only minor change of their oxidation state.[71] There is an additional storage site for Mg^{2+} with a charge transfer toward S (Mg^{2+} insertion in the inner ring), but this process suffers from intrinsically slow kinetics (see Figure 4b) and is fully accessible only at elevated temperature.[72] Replacing S with Se could retrieve the capacity from anionic redox, as is evident in the Mo_6Se_8 cathode.[73]

However, applying TM cluster compounds as cathode materials is a strategy that compromises Mg^{2+} mobility with specific capacity as well as voltage. The reduced capacity is attributed to the involvement of many heavy TM components in the cathode. On the other hand, redox reactions relying on metallic bonds generally provide low voltage, for example, considering an extreme case, that alloy compounds are used as anode.[75] In fact, the Chevrel phase Mo_6S_8 provided a practical capacity of ≈70 mAh g^{-1} at 1.1 V at room temperature.[7] Orthorhombic Mo_9Se_{11} is another cluster compound that delivered a reversible capacity of only ≈20 mAh g^{-1} at ≈1 V.[76] Shifting from chalcogenide to oxide clusters can theoretically increase the energy density, which still remains to be experimentally validated after being proposed now for more than 10 years.[77]

In an attempt to replace the TM with lighter elements, Zhang et al. reported fullerene (C_{60}) as Mg host, which provided an initial capacity of ≈50 mAh g^{-1}.[74] By using this highly conjugated carbon framework, the redox potential could be increased to 1.5 V versus Mg (see Figure 4c). This work demonstrated a possible improvement by using highly conjugated organic compounds. Note that, Mg^{2+} diffusion in organic compounds also benefits from their structural flexibility with large intramolecular spaces.[78] A detailed evaluation of the organic cathodes for Mg^{2+} will be presented in Section 4.

2.2.2. Simultaneous Cationic and Anionic Redox

Another approach to enable multi-center redox but do not rely solely on TM is to involve anionic redox in addition to the cationic
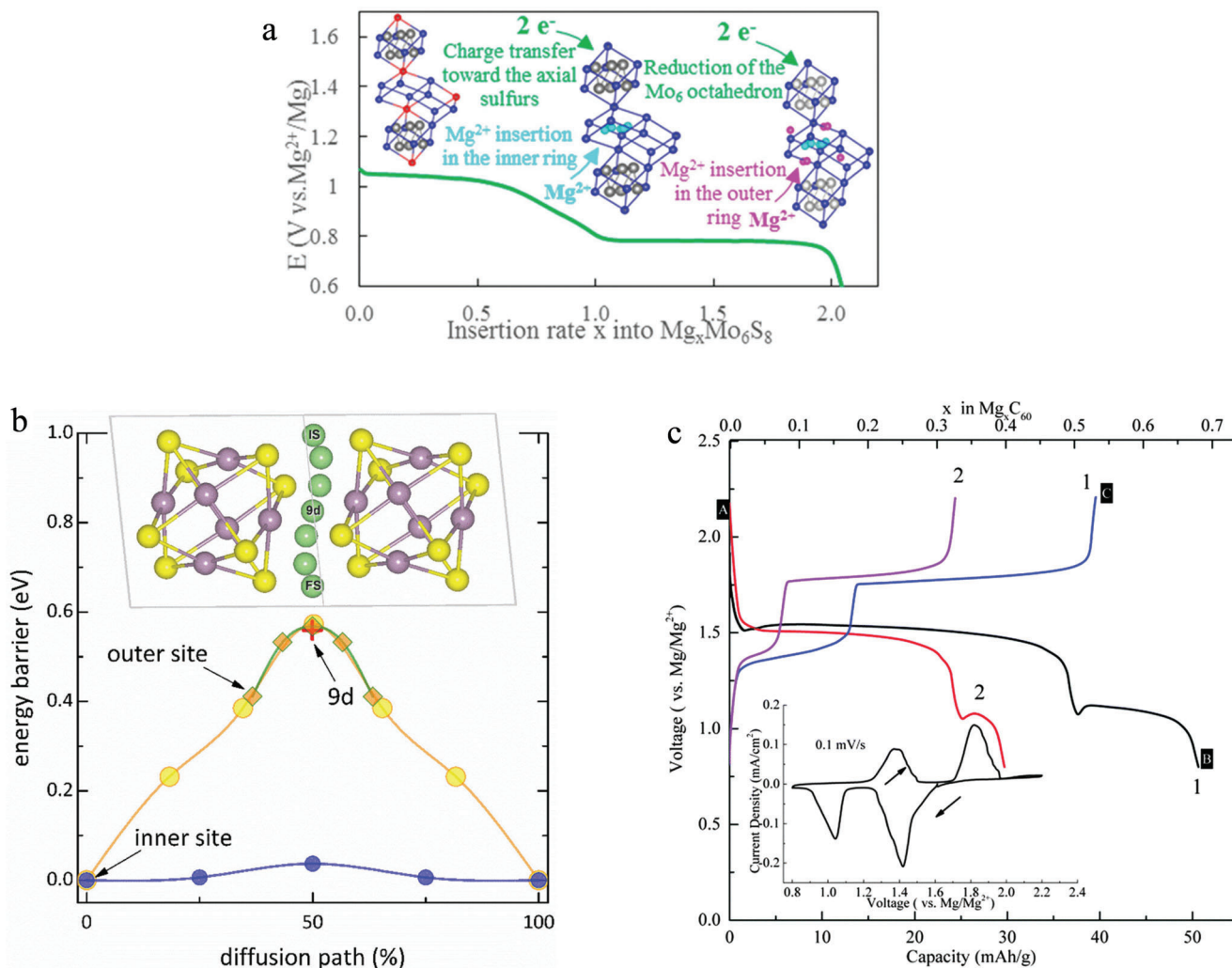
**ADVANCED
SCIENCE NEWS**

www.advancedsciencenews.com

**ADVANCED
ENERGY
MATERIALS**

www.advenergymat.de

Figure 4. a) Mg^{2+} insertion into Chevrel phase Mo_6S_8. Reproduced with permission.[71] Copyright 2017, American Chemical Society. b) Diffusion energy profile of Mg^{2+} at outer site (charge transfer toward S) and inner site (charge allocation to Mo_6 octahedron). Reproduced with permission.[72] Copyright 2017, American Chemical Society. c) Electrochemical performance of fullerene cathode for Mg. Reproduced with permission.[74] Copyright 2015, The Royal Society of Chemistry.

redox. Ideally, both cationic and anionic redox take place at a similar voltage, so that the extra charges could be allocated homogeneously on each redox center.[43] Simultaneous cationic and anionic redox (SCAR) can therefore be triggered in transition metal chalcogenide (TMC) compounds when valence orbitals of the TM overlap with the chalcogenide orbitals in the energy diagram.[68] The overlapping valence orbitals enable internal electron exchange, generating a delocalized electronic structure among the lattice frame as shown in **Figure 5**a. Moreover, unlike the classical ionic compound with TMs, the SCAR-based TMC compounds provide bondings with higher covalency.[42] In this way, the overall polarizability of the cathode structure is enhanced, resulting in a weaker interaction environment for Mg^{2+} diffusion.

Compared to S, Se provides larger 4p orbitals with higher energy, allowing more overlap with the TM bands.[80] In fact, orbital mixing was first demonstrated with a layered $TiSe_2$ cathode for Mg batteries.[43] Galvanostatic cycling of the micron-sized $TiSe_2$ cathode displayed a capacity of ≈120 mAh g^{-1}, which is

close to the theoretical value of 130 mAh g^{-1} based on Ti^{4+}/Ti^{3+} redox, with only slight decay after 50 cycles (Figure 5b). A negligible change of d-spacing from 6.01 to 6.07 Å after 0.5 Mg^{2+} intercalation was revealed by ex situ XRD measurement, indicating a weaker interaction between the shuttling ion and the cathode. A similar Mg storage performance was further confirmed in a VSe_2 cathode,[42,43] indicating potential kinetic advantages of the selenide compounds.

In order to reach a higher voltage and be more sustainable, efforts were made to extend this approach to TMSs.[81,82] The SCAR chemistry is therefore conceptualized in a VS_4 cathode, where S is in a dimer form (S_2^{2-}), which enables orbital mixing.[68] The cathode delivered a reversible capacity of 330 mAh g^{-1} (≈1.2 Mg^{2+}) at 100 mA g^{-1} for 20 cycles in a tetrakis(hexafluoroisopropyloxy)borate $Mg[B(hfip)_4]_2$-based electrolyte (Figure 5c), despite a considerable decay in the long-term cycling. Interestingly, DFT analysis suggested that the disulfide groups, which bridge the adjacent V, not only participate in the
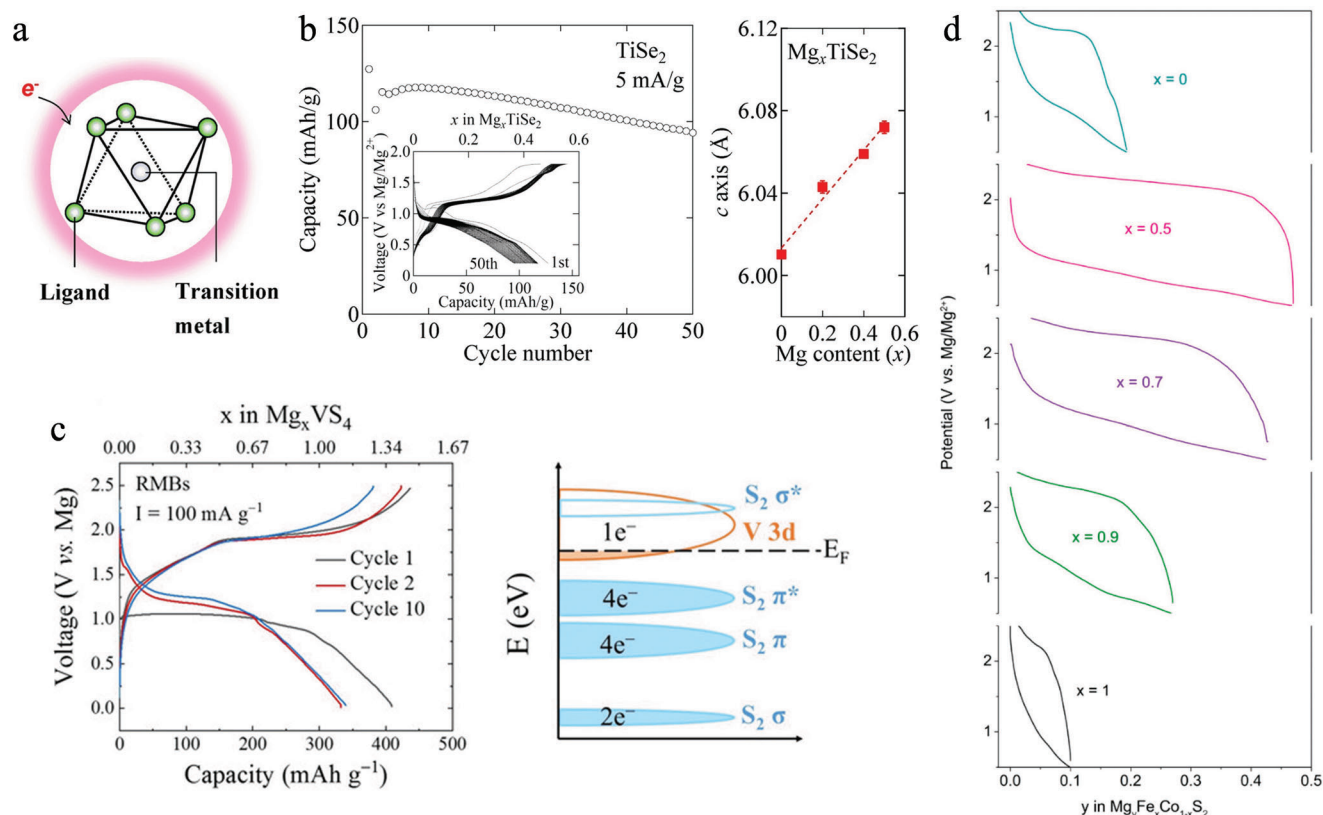
ADVANCED
SCIENCE NEWS

www.advancedsciencenews.com

ADVANCED
ENERGY
MATERIALS

www.advenergymat.de

Figure 5. a) Schematics show delocalized electronic cloud among transition metal–ligand compounds. b) Cycling of $TiSe_2$ against Mg and the corresponding change of d-spacing upon Mg intercalation. Reproduced according to the terms of the CC BY license.[43] Copyright 2015, The Authors, published by Springer Nature. c) Mg storage in VS_4 (left) and the band structure of VS_4 (right). Reproduced according to the terms of the CC BY license.[68] Copyright 2020, The Authors, published by Wiley VCH. d) Electrochemical performance of $Mg_yFe_xCo_{1−x}S_2$. Reproduced with permission.[79] Copyright 2020, American Chemical Society.

redox, but also actively support Mg^{2+} transport by flexible adjustment of their position.[68] Other TMSs with disulfide groups such as CoS_2 and FeS_2 were also investigated. While each individual compound could only host limited amount of Mg^{2+}, a cationic doping gave rise to a considerable improvement of the capacity as presented in Figure 5d.[79] With highly reversible cationic (Fe and Co) and anionic (S) redox, the optimized $Fe_{0.5}Co_{0.5}S_2$ cathode delivered a stable capacity of 154 mAh g$^{−1}$ after 100 cycles. Further improvement in the capacity to 175 mAh g$^{−1}$ was achieved in an amorphous TiS_x material, but only at an elevated temperature of 60 °C.[83]

When shifting from selenide to sulfide, reversibility of the SCAR chemistry seemed to be reduced. A mechanistic investigation of VS_4 upon de-/magnesiation pointed out a parasitic conversion reaction. This deteriorates the crystal structure and takes place at a similar voltage as the insertion process.[84] As side products such as V^0 and MgS forms, the Coulombic efficiency of the system may be severely influenced. Therefore, it remains challenging for the SCAR-based compounds to involve anionic redox with a small structural deformation, and this is also an uncharted territory. On the other hand, the electrophilic disulfide groups might raise concern of the cathode–electrolyte compatibility.[80] As most of Cl-based Mg electrolyte are nucleophilic, a proper selection of electrolyte could clarify the issue.

2.3. Screen the Double Charge of Mg^{2+}: Cointercalation

Apart from the cathode structures, strategies aiming at screening the high charge density of Mg^{2+} were also developed. These strategies focused mainly on the establishment of new intercalation chemistries, which involved an assisting agent that cointercalates with Mg^{2+}. Alternatively, attempts were also made by functionalizing the diffusion tunnels of the host structures with some of those shielding agent. In order to reduce the overall charge density of the Mg-based intercalants, the assisting agent can be either anions (such as $Cl^−$),[22] which reduce the net charge, or small molecules (e.g., H_2O and DME)[85,86] that increase the total volume of the cations.

2.3.1. Intercalation of $MgCl^+$

$Cl^−$ ions greatly enhance the ion transport of various Mg electrolyte by promoting their dissociation with the formation of electrochemically active $Mg_xCl_y^+$ species.[87,88] Compared to Mg^{2+}, these $Mg_xCl_y^+$ species are monovalent cations with a larger size, resulting in a much smaller charge density. Therefore, these Mg–Cl multimeric clusters exhibit faster solid diffusion kinetics, among which $MgCl^+$ is thermodynamically most stable and
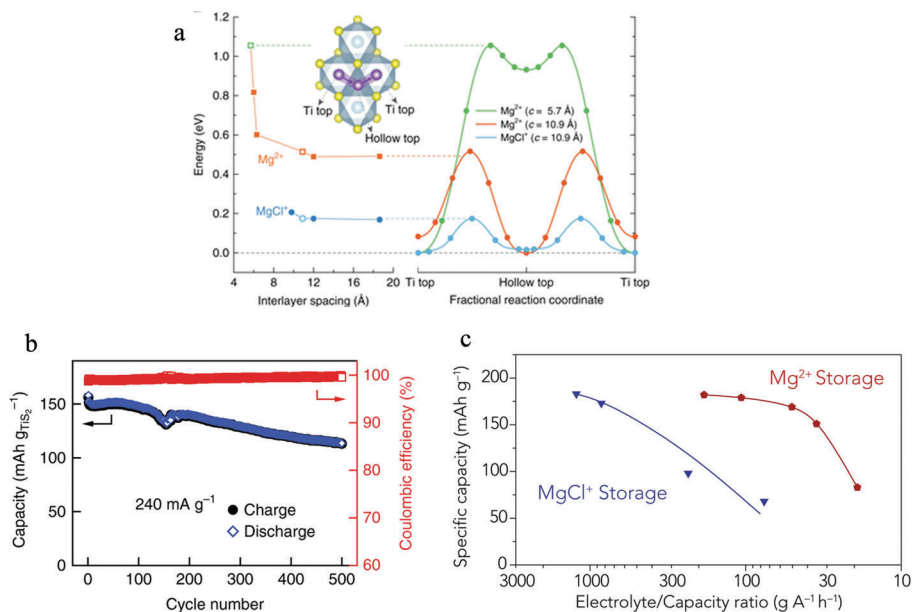
**ADVANCED
SCIENCE NEWS**

www.advancedsciencenews.com

**ADVANCED
ENERGY
MATERIALS**

www.advenergymat.de

Figure 6. a) Energy profiles for Mg^{2+} and $MgCl^+$ diffusion in TiS_2 with different interlayer spacing. b) Cycling performance of expanded TiS_2 with $MgCl^+$ intercalation. Reproduced according to the terms of the CC BY license.[22] Copyright 2017, The Authors, published by Springer Nature. c) A comparison of electrolyte required with Mg^{2+} and $MgCl^+$ storage. Reproduced with permission.[91] Copyright 2019, Elsevier.

smallest in size.[89] As reported, replacing Mg^{2+} with $MgCl^+$ intercalation into an interlayer-expanded TiS_2 ($d = 10.9$ Å) led to a drastic reduction of diffusion barrier from 0.51 to 0.18 eV (**Figure 6**a), corresponding to more than five orders of magnitude higher diffusivity.[22] Notably, the $MgCl^+$-based intercalation chemistry also enhanced the interfacial reaction kinetics by circumventing the Mg–Cl dissociation, which is energetically unfavorable (kinetic barrier > 3 eV).[90] With this synergetic effect, $MgCl^+$ storage in a pillared TiS_2 provided a capacity of 150 mAh g^{-1} at 240 mA g^{-1} for 500 cycles (Figure 6b).[22]

To accommodate the larger cations without severe steric effect, an expanded structure seems to be a prequisite to enable Mg–Cl cointercalation. Such a structure can be obtained either by crystal engineering during material synthesis[92] or via in situ formation during initial cell cycling with pillar agent as additive in the electrolyte.[61] The latter approach seems more practical and additional synthetic steps for structural expansion can be avoided. However, attention should be paid on the selection of the pillars as electrolyte additives, as they should have minimal impact on the equilibria in the Cl-based electrolyte.[14] Additionally, although $MgCl^+$ intercalation was reported in a $VOPO_4$ cathode,[63] applying the approach in high-voltage oxide materials remains questionable. The corrosive nature of Cl^- raises compatibility issues with metal oxides.[17] Another limitation of the $MgCl^+$ cointercalation process is the consequence of low specific energy at cell level. Particularly under lean electrolyte conditions, the specific energy of systems with $MgCl^+$ storage might be reduced by 2/3 when compared to the Mg^{2+} storage (see Figure 6c).[91]

2.3.2. Intercalation of Solvated Mg^{2+}

Solvent molecules with highly polarizing groups (such as O-containing groups) coordinate strongly with Mg^{2+}. With the in-

tercalation of solvated Mg^{2+}, the solvation shell can effectively shield the double charge of Mg^{2+} ions and thereby reduce their electrostatic interactions with the host lattice. Water is the smallest molecule that contains O. It was found that the electrochemical performance of various oxide materials improves with the H_2O content in Mg electrolytes.[86,93] The capacity increase was impressive as reported in MnO_2, which provided a stable capacity of >200 mAh g^{-1} at ≈2.6 V versus Mg in an electrolyte with 10 м H_2O.[86] On the down side, water is stable only within a narrow electrochemical window of 1.23 V, making it challenging for building Mg batteries with high cell voltage.[94] Beyond that, protons would be generated by the hydrolysis of water, which is also a common side reaction in aqueous batteries that contributes to the overall capacity. In extreme cases, proton shuttling might prevail over Mg^{2+} intercalation even in dry electrolyte conditions.[95] Therefore, a careful interpretation of the electrochemical performance by combining elemental, redox, and structural analysis is necessary.[96] A thorough understanding of the storage mechanism would be beneficial for further developing strategies that allow dominant hydrated Mg^{2+} intercalation by suppressing the proton shuttling.

A more practical concern on the water-containing electrolyte is their incompatibility with Mg metal anode.[97] This issue could be alleviated by involving crystal water as pillar in the cathode structure, for example, $Mg_{0.3}V_2O_5·1.1H_2O$.[98] However, due to the strong interaction between Mg^{2+} and water molecules, the stability of the hydrated structures and their compatibility with metal anode upon repeated de-/magnesiation requires further experimental validation. To reproduce the favorable behavior of hydrated Mg^{2+}, organic solvent molecules with similar physicochemical features are promising. This strategy is previously impeded in the Cl-based electrolytes where close coordination between Mg^{2+} and solvent was hindered by strong Mg–Cl interaction.[14] The development of Cl-free simple-salt Mg
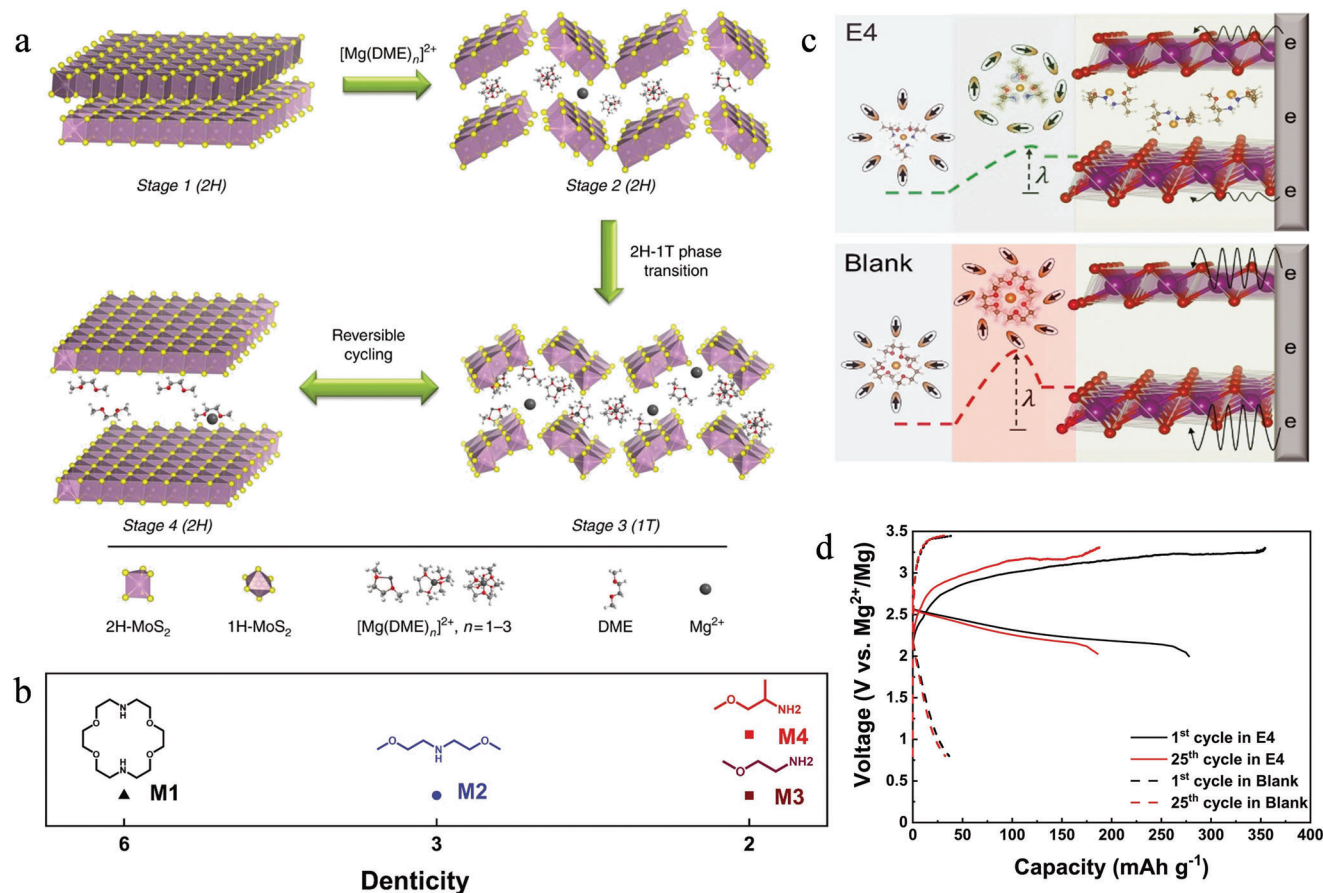
Figure 7. a) Schematics of $[Mg(DME)_3]^{2+}$ intercalation into an expanded MoS_2 structure. Reproduced with permission.[20,85] Copyright 2018, The Authors. b) Some typical methoxyethylamines. c) A scheme shows the effect of solvation structure on Mg intercalation. d) Voltage profiles of $Mg–Mg_{0.15}MnO_2$ cell with and without methoxyethylamine additive. Reproduced with permission.[20,85] Copyright 2021, The Authors, published by AAAS.

electrolytes paved the way for the intercalation of solvated Mg^{2+} ion, which is readily available in the electrolyte.[99] Initial effort was made in graphite with a flexible molecular layers.[100] Thermodynamically, Mg^{2+} dose not intercalate into graphite, but forms a trinary compound with glyme-based solvent in graphite. Although the cointercalation process was both thermodynamically and kinetically favorable, the large size of the solvated ions led to significant expansion of the host structure, leading to amorphization of the graphite layers.[100]

Similar to graphite, 2D TMS also has a flexible layered structure. Intercalation of $Mg(DME)_3^{2+}$ into an expanded MoS_2 structure was demonstrated in a $Mg[B(hfip)_4]_2$/DME electrolyte (**Figure 7**a).[85] Multimodal characterizations by means of 4D-STEM and XPS confirmed the de-/intercalation of Mg^{2+} together with DME, accompanied by a phase transition from thermodynamic stable $2H-MoS_2$ to metallic $1T-MoS_2$, with enhanced charge transfer. Furthermore, the phase transition with certain structural distortion was found beneficial for hosting solvated Mg^{2+}, resulting in a capacity of 120 mAh g^{-1} for 100 cycles.[85]

Inspiringly, further applying this strategy in high-voltage oxides was recently reported.[20] The success of solvated Mg^{2+} intercalation into a layered $Mg_{0.15}MnO_2$ was enabled by a proper design of the solvation structure in the electrolyte. It was discov-

ered that methoxyethyl-amines (Figure 7b) with tailored chain length provided a less compact coordination to Mg^{2+} with heterogeneous donor atoms. The flexible solvation structure allowed adjustable configuration with a low reorganization energy for intercalation into the layered oxide (see Figure 7c). By coupling with a Mg anode, the cell delivered a high capacity of 190 mAh g^{-1} with cell voltage of 2.4 V (Figure 7d), amounting to an energy density of 412 Wh kg^{-1}.[20] The promising result highlighted another merit of the cointercalation strategy, to push the thermodynamic limit by establishing ternary intercalation chemistries based on Mg.

3. Promoting Charge Transfer at Cathode–Electrolyte Interfaces

As mentioned before, cointercalation strategies also address interfacial issues related to dissociation (in the Cl-based electrolyte) and desolvation (in the Cl-free electrolyte) of Mg-based cations.[22,85] According to DFT calculation, the energy barrier for breaking the Mg–Cl bonds can be twice higher than that for Mg^{2+} diffusion within layered TiS_2.[22] Similarly, desolvation energies for Mg^{2+} are also more than twice as for Li^+ in various organic solvents.[101] These results indicate that interfacial charge trans-
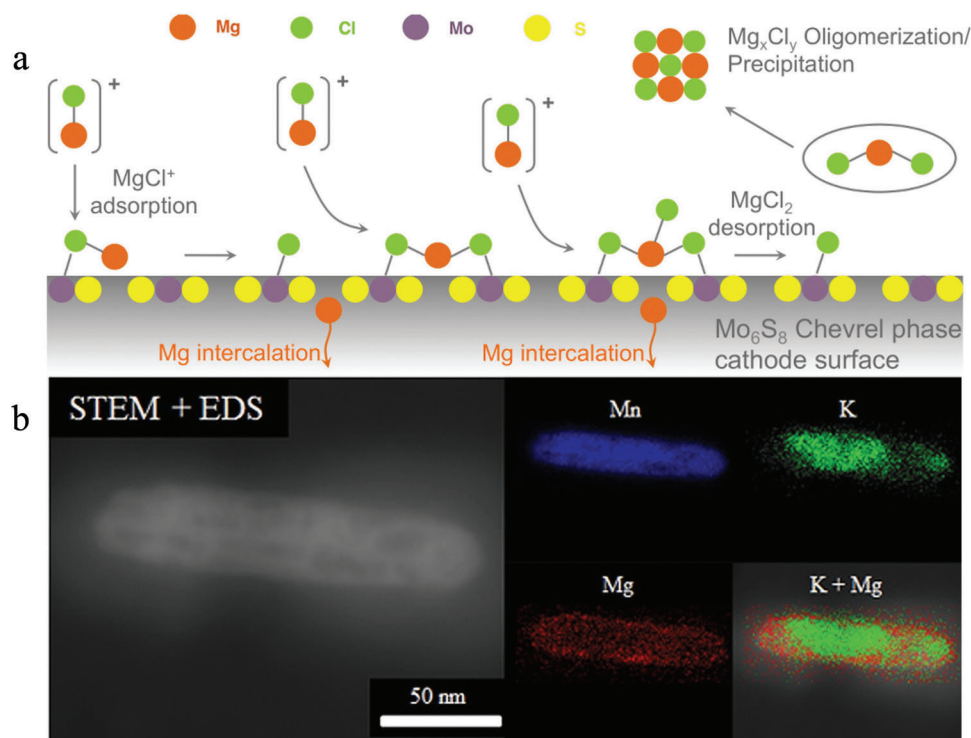
Figure 8. a) Schematics showing Mg intercalation into the Chevrel phase Mo_6S_8 in a Cl-based electrolyte. Reproduced with permission.[90] Copyright 2015, American Chemical Society. b) STEM-EDS of a K-contained α-MnO_2 after magnesiation. Reproduced with permission.[33] Copyright 2014, American Chemical Society.

fer in Mg batteries might be a rate-determining step rather than solid diffusion. While the interfacial issue is well-recognized for Mg anode, the cathode interfaces with more complex processes is still an emerging field that deserves more attention.[17,102]

3.1. Cathode Interfacial Phenomena in Mg Batteries

With such a high dissociation energy, the first question came to mind is why the Chevrel phase Mo_6S_8 exhibits an excellent cycling stability in the APC electrolyte.[7] Therefore, a detailed study was conducted on the interfacial processes and intercalation mechanisms of the Mo_6S_8 upon magnesiation.[90] It was learnt that the (100) surface of Mo_6S_8 serves as a catalyst for promoting the dissociation of the Mg_xCl_y species (**Figure 8**a). The surface exposed Mo atoms could reduce the activation energy sharply from 3 to 0.2 eV, by interacting with Cl atom in the Mg_xCl_y clusters.[90] Considering the critical role of Cl^- in the plating/stripping of Mg anode, the outstanding Mg storage performance of Chevrel phase Mo_6S_8 seemed to rely on the Cl-based electrolyte.[17,103]

However, it does not necessarily mean the insertion of Mg^{2+} in the Mo_6S_8 cathode from a Cl-free electrolyte is impossible.[104] This argument was experimentally validated with the $Mg[B(hfip)_4]_2$/DME electrolyte, in which the Chevrel phase Mo_6S_8 cathode delivered a stable capacity of 65 mAh g^{-1} at 50 mA g^{-1} for more than 600 cycles.[105] In fact, the dissociation of Mg compounds in the Cl-free electrolyte with weakly coordinating anions (WCAs) is supported by the ethereal solvent

molecules, which have weaker coordinating strength than Cl^-.[14] In general, desolvation process in the Cl-free electrolyte to break the Mg–O (solvent) bond should be energetically more favorable than Mg–Cl dissociation in the Cl-based electrolyte. Nevertheless, a thorough understanding of the magnesiation processes as well as interfacial processes in the Cl-free electrolyte is still pending, which would allow a direct comparison with those in the Cl-based electrolyte.

Another advantage of the Chevrel phase Mo_6S_8 associated with its superior ionic conductivity is that it allows bulk diffusion even in micron-sized particles at room temperature.[106] Unfortunately, this is an exceptional case among the discovered cathode materials for Mg batteries. In most cathode hosts, the sluggish diffusivity of Mg^{2+} limits its penetration depth into the cathode bulk, forming a core–shell structure in large particles. Due to relative high Mg^{2+} content in the surface region, undesired interfacial processes could take place. An amorphous layer was reported on the surface of α-MnO_2 cathode (see Figure 8b), consisting mainly the conversion products.[33] A similar layer was found on olivine $FePO_4$, where Mg^{2+} insertion led to strong structural distortion, and thereby surface amorphization.[47] In both cases, the amorphous layer, even with a thickness of few nanometers, could already prevent further electrochemical reactions into the depth, resulting in a low capacity.

Due to the limited penetration depth of Mg^{2+}, size effect is prominent in most of the cathode materials, even in sulfide cathodes with moderate voltage.[107] To fully extract the electrochemical performance and to reach a more homogeneous magnesiation state, reducing particle size is a feasible approach.[108] At the

expense of volumetric density, this strategy promotes the discovery and the development of new compounds for Mg storage.[109] While such strategies allow a better evaluation of the Mg hosts, attention should be paid on more severe side reactions due to larger surface area. In the form of nanoparticles, materials generally have higher (electro-)chemical reactivities, also to other cell components that supposed to be inert.[110] As the side reactions could contribute to the measured capacity, careful evaluation is required for these materials and their possible interphases. To the best of our knowledge, studies of cathode–electrolyte interphases remain largely unexplored in Mg batteries.[111]

3.2. Enhancing the Cathode–Electrolyte Compatibility

To enable a reversible cathode chemistry in Mg batteries, a proper electrolyte selection is crucial. The choice of electrolyte should also consider the compatibility with Mg metal anode, which enables high-energy full-cells. However, metallic Mg readily forms surface passivating film consisting MgO and Mg(OH)$_2$ etc. even after fresh polishing under protective atmosphere. To get rid of the native passivating layer, aggressive electrolytes mostly containing Cl-based Lewis acidic moieties were applied, serving as scavengers.[17] The scavengers that are capable of removing the oxide layer should in principle also react with other oxide materials, for example, oxide cathodes.[16] In fact, their nucleophilic nature further limits their chemical compatibility with electrophilic electrodes that contain S−S bonds or redox-active organics, which are widely investigated in the community.

To this end, the development of new electrolyte with enhanced electrochemical stability as well as chemical stability is highly demanded, among which non-nucleophilic Mg compounds that do not contain Cl components attracted most attention. In search for suitable anions, Mg(BH$_4$)$_2$ was first reported, however with limited anodic stability of $\approx$2 V versus Mg.[112] As Mg^{2+} is highly polarizing, bulky anions with monocharge were proposed that weaken the interaction with Mg^{2+} via delocalized electrons. Further taking into account the oxidative stability led to the design of carborane anions[104] and fluorinated alkoxyborates,[99] both provided electrochemical windows up to 4 V versus Mg, and exhibit excellent Mg plating/stripping efficiency. Simple-salt Mg compounds with WCAs represent a new research direction toward more practical Mg electrolytes that can be benchmarked for the evaluation of high-voltage cathode materials.

In addition to anions, the solvent choice is another decisive factor when it comes to cathode–electrolyte compatibility. It does not seem to be a major concern in LIBs, due to the use of carbonate solvent which is stable at high voltages. However, solvents that have been experimentally validated to support reversible Mg plating/stripping are only ethers, whose oxidative stability is only up to $\approx$3.5 V versus Mg as free molecules.[17] Indeed, the electrochemical window of ether-based electrolyte can be extended either kinetically or via coordinating with Mg^{2+}. Even though, these intrinsic properties of ethereal solvent would raise concerns on the stability during long-term cycling, which becomes even critical in more practical lean-electrolyte conditions. Screening more suitable solvent for Mg batteries is challenging as a lot of crossover issues have to be addressed in parallel. However, recent

findings with cosolvents for Mg batteries may serve as a guideline for further discovery of solvent beyond ethereals.[20]

To enhance the cathode–electrolyte compatibility, efforts were also made to introduce protective layer on the cathode materials that separate the cathode chemistry from the electrolyte.[113] A successful development of the strategy allows the use of electrolytes that are otherwise incompatible with the cathode materials. The protective layer can be formed in situ by partial electrolyte decomposition during battery cycling, typically known as cathode electrolyte interphase (CEI) in LIBs. As such interphases developed in Mg electrolytes have been found mostly passivating to Mg^{2+}, identifying suitable CEI components for Mg cathodes is challenging. Thus, designing well-functioning CEI layers through optimization of electrolyte formulation is still a small, but emerging field and may yield fast interfacial transport to support subsequent bulk diffusion in the cathode.[114]

Alternatively, a protective layer could also be developed artificially by coating onto the particles of cathode materials. An ideal cathode coating should be chemically inert to the electrolyte, but also conduct Mg^{2+} and be electrochemically stable at the operating voltage window. Concerning the sluggish solid diffusion of Mg^{2+}, applying combinatory kinetic strategies to coating materials with high (electro-)chemical stability may be more feasible. Such strategies include controlling the thickness of the coating, building a porous coating layer, or introducing vacancies that allow Mg hopping.[115] As predicted by DFT calculations, MgF$_2$, Mg(PO$_3$)$_2$, and MgP$_4$O$_{11}$ could be promising candidates for protecting high-voltage cathode materials from electrolyte degradation.[113]

3.3. Optimizing the Solvation Structure of Mg-Ions

While cointercalation strategy circumvents the desolvation/dissociation processes at interfaces, another approach to tackle the interfacial issue is optimizing the solvation structure of Mg in the electrolyte to lower the energy barrier for desolvation. In view of the solvation environment in an electrolyte solution based on a single Mg compound, anions and solvents are competing in coordinating with Mg^{2+} (**Figure 9**a).[14] Therefore, a trade-off has to be made between easier desolvation and adequate dissociation with the main anions, which guarantees sufficient ion transport in the electrolyte. Achieving this goal requires optimization of the electrolyte formulation, for example, by a proper design of the main anions, a fine selection the solvent, or the introduction of additives. Investigations on the solvation structure of Mg^{2+} that have been carried out so far are mostly targeting at more reversible anode reactions.[20,116,117] However, if successfully developed, these strategies could also promote interfacial processes at cathode, as the desolvation of Mg^{2+} is important for cathode chemistry as well.

The solvent effect on the intercalation of Mg^{2+} was investigated with a thin-film V$_2$O$_5$ electrode in a Mg(ClO$_4$)$_2$-based electrolyte.[40] It was found that acetonitrile (ACN) has a low solvation energy, enabling reversible Mg^{2+} intercalation into the V$_2$O$_5$ cathode from the Mg(ClO$_4$)$_2$/ACN electrolyte (Figure 9b). However, the charge transfer across the cathode interface was impeded by the presence of DME even in a small amount, which already led to the formation of more stable Mg(DME)$_3$$^{2+}$ ions with

ADVANCED
SCIENCE NEWS
www.advancedsciencenews.com

ADVANCED
ENERGY
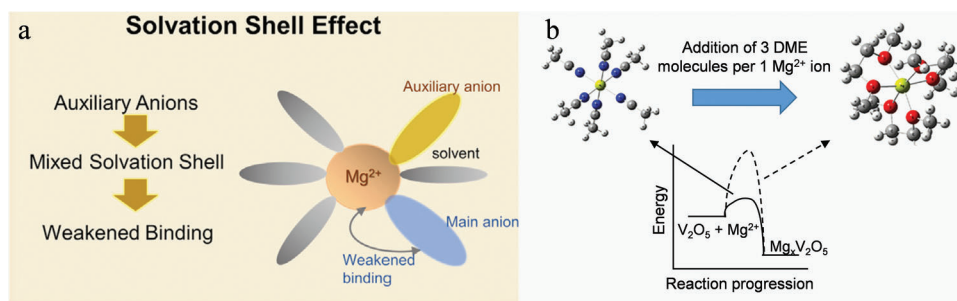**MATERIALS**
www.advenergymat.de

Figure 9. a) Solvent and anions are competing in coordinating to Mg^{2+}. Reproduced with permission.[14] Copyright 2020, Elsevier. b) Change of the solvation structure in the $Mg(ClO_4)_2$/ACN electrolyte with the addition of DME. Reproduced with permission.[40] Copyright 2018, Wiley.

much higher desolvation barrier. This result could explain why various cathode materials exhibited promising electrochemical performance in the ACN-based electrolyte, but failed to be transferred to full-cell configurations against Mg metal anode with a DME-based electrolyte.[118]

From practical perspective, ethers are the only type of solvent discovered so far that enables reversible Mg plating/stripping. Although a direct comparison of Mg^{2+} insertion from different glyme-based electrolytes is still pending, investigation of the desolvation pathways at Mg anode may provide guidelines for a similar process at cathode interface. Therefore, a recent study highlighted desolvation as a limiting step for Mg deposition in Cl-free electrolytes.[117] To break the compact solvation structure, the initial desolvation of Mg^{2+} in $Mg[B(hfip)_4]_2$/glyme electrolytes to free the first coordination site was found the most energy intensive process. Tackling this issue, cosolvents that have strong chelating groups but form more flexible solvation sheath with DME were proposed (see Figure 7c), exhibiting excellent interfacial charge transfer properties at both cathodes and anodes.[20,119] In addition to solvents, electrolyte additives could also regulate the solvation structure by providing auxiliary anions. A fine tuning can be achieved by balancing out the relative association strengths between the main anions and the auxiliary anions that generate cooperative effect for fast cathode reactions.[116] Overall, further efforts in this research direction can be devoted to the development of novel electrolyte and the discovery of co-/solvent or electrolyte additives for Mg batteries.

4. Systems That Circumvent Ion Diffusion in Ionic Crystals

As the diffusivity of Mg^{2+} in solids is rather limited, strategies that bypass its de-/insertion processes in rigid crystal structures at the cathode, yet still allowing the implementation of a metallic Mg anode, could be a game changer. Bulk diffusion of the divalent charge carriers can be circumvented by triggering heterogeneous redox reactions at the cathode–electrolyte interfaces, including mainly the Mg–S (Se) chemistry,[120] but also the emerging enolization reaction in small molecular organic compounds.[9] Therefore, their Mg storage performance heavily depends on the use of a conductive matrix, wherein the active material is homogeneously loaded. As charge transfer is mostly attributed to interfacial reactions, fast redox kinetics can be guaranteed. A major challenge of the cathode with heterogeneous reactions is the formation of soluble intermediates, which leak

into the electrolyte, limiting the reversibility of the cell. Targeting this issue, redox active polymers were developed, exhibiting fast-charging capability in Mg batteries.[121] The coordinating polymers allow fast Mg storage by offering molecular chains with weak intramolecular forces, which enables easy access of Mg^{2+} from the electrolyte. The ionic mobility can be further enhanced by the segmental motion of the flexible chain-like structures, which is energetically favorable for both intermolecular and intramolecular hopping.[78] Besides, approaches were also established by completely getting rid of Mg^{2+} storage at the cathode side. Typical examples are hybrid or dual-ion systems that incorporate the shuttling of monovalent ions at cathode side and the redox of Mg at anode, both of which have fast redox kinetics.[122]

4.1. Heterogeneous Redox Systems: Sulfur, Selenium, and Iodine Cathodes

Enabling liquid phase redox reactions is an obvious approach to circumvent the diffusion restrictions of divalent ions in solids. Despite providing this advantage, these soluble active species face the challenge of migration from the cathode matrix and redistribution in agglomerates. The mechanisms and approaches to overcome these issues are pointed out in the following.

4.1.1. Sulfur Redox System

Conversion-type materials and compounds, which do not (solely) rely on ion diffusion within the crystal lattice, are suitable alternatives to intercalation cathodes—with sulfur being the most popular representative due to its high capacity and abundance. However, its low electric conductivity of 10^{-28} S m^{-1} requires a conductive host, wherein sulfur agglomerates with large thickness have to be avoided to enable fast sulfur redox reactions (**Figure 10**).

The most popular host materials are carbons, which combine high electric conductivity with high surface area. Thus, in recent years, many different carbon-based materials like amorphous mesoporous carbon (AMC),[124] Ketjenblack,[125] activated carbon cloth (ACC),[123,126–128] CMK3,[129,130] rGO,[131] N-doped graphene,[132] CNT,[124] MWCNT,[133] and MWCNT + graphene[134] were utilized in Mg–S batteries. To achieve a uniform sulfur distribution therein, different approaches like mechanical intrusion, liquid impregnation, melt,
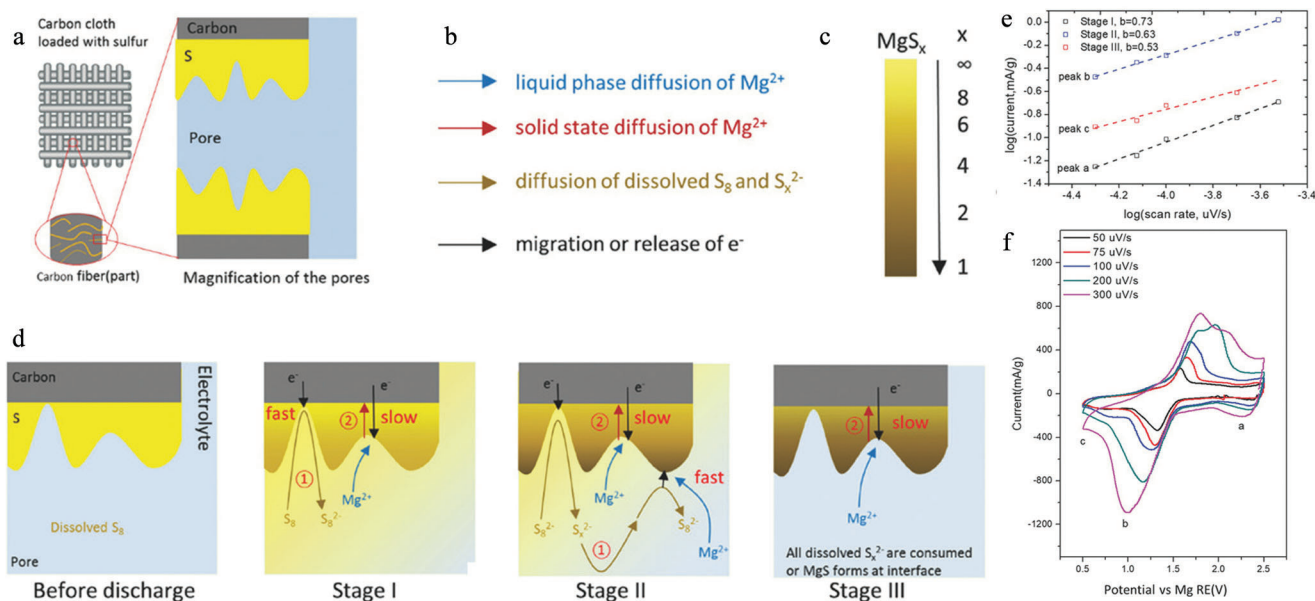
**ADVANCED
SCIENCE NEWS**

www.advancedsciencenews.com

**ADVANCED
ENERGY
MATERIALS**

www.advenergymat.de

Figure 10. a–d) Schematic reduction mechanism of a sulfur/carbon composite cathode (exemplarily ACC/S) with the different kinetic processes occurring during the three stages of discharge. e) CV of Mg–S cells at different scan rates and f) the corresponding kinetic fitting of the peak current ($i = av^b$, with i: peak current density, v: scan rate). Reproduced with permission.[123] Copyright 2017, Wiley.
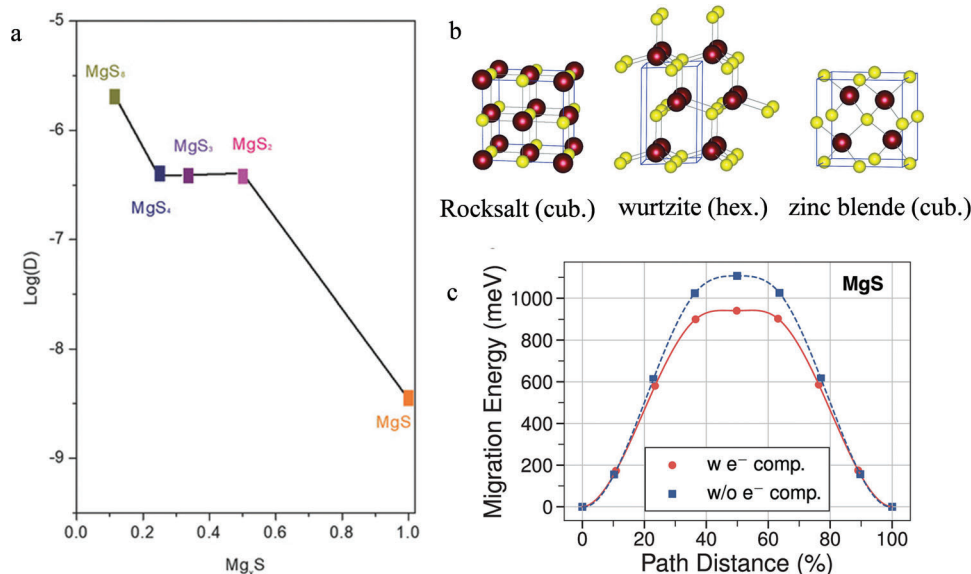
Figure 11. a) AIMD-calculated diffusion coefficient for Mg^{2+} in MgS_x ($x = 1–4$ and 8) at 600 K. Reproduced with permission.[123] Copyright 2017, Wiley. b) The three different crystal structures of MgS with the cubic rocksalt structure being the thermodynamically most stable. Reproduced with permission.[138] Copyright 2017, International Union of Crystallography. c) AIMD-calculated migration barrier for Mg^{2+} ions along the migration paths in MgS (943 meV). Reproduced with permission.[139] Copyright 2019, American Chemical Society.

or vapor infiltration were applied in the past decade. However, due to the solubility of sulfur and especially polysulfides, redistribution of sulfur species during cycling may occur, resulting in large agglomerates, blocking of conductive surfaces, and an active material gradient toward the current collector.[135,136]

Besides the slow migration of electrons, the solid-state diffusion of Mg^{2+} within carbon, sulfur, and magnesium sulfide is also sluggish (**Figure 11**a). Consequently, the kinetic characteristics along discharge differ due to the reaction in liquid and solid phase and the changing environment within the cathode. While in Stage I/II both, surface and bulk magnesiation occurs to result in mixed kinetics, Stage III only involves bulk magnesiation with diffusion-controlled kinetics (Figure 10d–f). While the diffusivity in amorphous MgS_2 is still sufficient, it significantly drops, when crystalline MgS is formed—either in hexagonal wurtzite structure (hcp)[133] or cubic structures (fcc) like zinc-blende[134,137] and
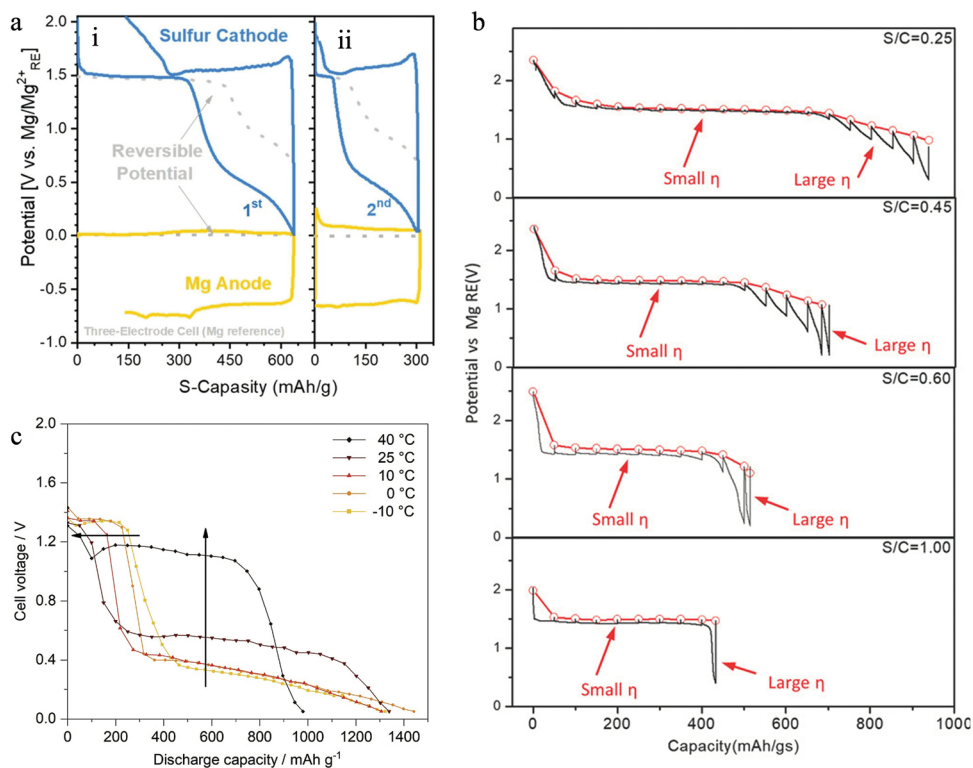
**ADVANCED
SCIENCE NEWS**

www.advancedsciencenews.com

**ADVANCED
ENERGY
MATERIALS**

www.advenergymat.de

Figure 12. a) Voltage profile of a Mg–S cell with Mg-reference electrode during (i) first and (ii) second discharge–charge cycle. The dotted line reflects the quasi reversible potential during GITT measurement. Reproduced with permission.[144] Copyright 2021, Wiley. b) Discharge and GITT curves with different S/C ratios. Reproduced with permission.[123] Copyright 2017, Wiley. c) Discharge (C/20) and GITT curves at different temperatures. Reproduced with permission.[125] Copyright 2020, Elsevier.

rock-salt.[138] While wurtzite and zinc blende exhibit tetrahedral coordination of Mg^{2+} cations, the rocksalt structure represents the thermodynamically most stable and dense structure with Mg^{2+} octahedrally coordinated by S^{2-}, which results in hampered reoxidation and Mg^{2+} diffusion, respectively (Figure 11b). This is in line with the calculated high migration barrier for Mg^{2+} ions in Mg-chalcogenides (Figure 11c), that correlates with the bandgap (migration barrier/bandgap in eV): MgO (1.851/6.02) > MgSe (0.95/3.00) > MgS (0.943/2.94) > MgTe (0.939/2.79).[139] Despite the ab initio predictions of wurtzite and zinc blende exhibiting 3.4 and 12.2 meV/atom higher formation energy than the rock-salt lattice, both structures are found at the end of discharge,[133,134,137] which might be beneficial in subsequent reoxidation.

The slow solid-state diffusion becomes even more crucial as the solubility of MgS_x species in non-polar solvents like THF or glymes is two orders of magnitudes lower (<50 mM) compared to their lithium counterparts.[140–142] Thus, the sulfur utilization and capacity gain in Mg–S cells is low and the redox reactions—especially the liquid–solid conversion during discharge and the subsequent solid–liquid conversion during charge—exhibit slow kinetics and provoke large overpotentials (**Figure 12**a,b). Due to the ionic diffusion being a thermally activated process[22,143] and the polysulfide solubility being enhanced with temperature, the average discharge potential is significantly increased at higher temperature[125] (Figure 12c). Therefore, in contrast to publications solely blaming the Mg anode for the cell

overpotential,[141] the cathode also contributes to overpotentials in significant manner.[144] Indeed, the Mg deposition is dominating the charge overpotential, yet it remains constant[141] or is even declining[128]—at least with Li electrolyte additives (**Figure 13**). The discharge overpotential, however, is governed by the sulfur reduction, especially in the final stage (Figure 13b) due to above-mentioned reasons. With the redistribution and agglomerates in mind, an increase of these overpotentials with cycle number is likely.

4.1.2. Selenium and Se–S Mixtures

Selenium is another conversion material under research due to its higher electric conductivity compared to sulfur (1×10^{-3} vs 5×10^{-28} S m^{-1}) at similar volumetric capacity (3265 vs 3459 mAh cm^{-3}).[145] However, there are also drawbacks like the lower cell voltage and lower gravimetric capacity (680 vs 1675 mAh g^{-1}) as well as its toxicity and higher raw material cost.

The redox processes in a Mg–Se cell follow a similar pathway compared to their sulfur analogues,[146] also forming soluble intermediates, that is, polyselenides ($MgSe_n$, $n \geq 4$), while a higher utilization of active material is achieved due to the higher electrical conductivity. Due to latter, the Se/CMK3 cathode offers a lower voltage hysteresis and better rate capability compared to a S/CMK3 cathode—however at a lower discharge voltage (note the elevated temperature of 50 °C in this study).[145] A
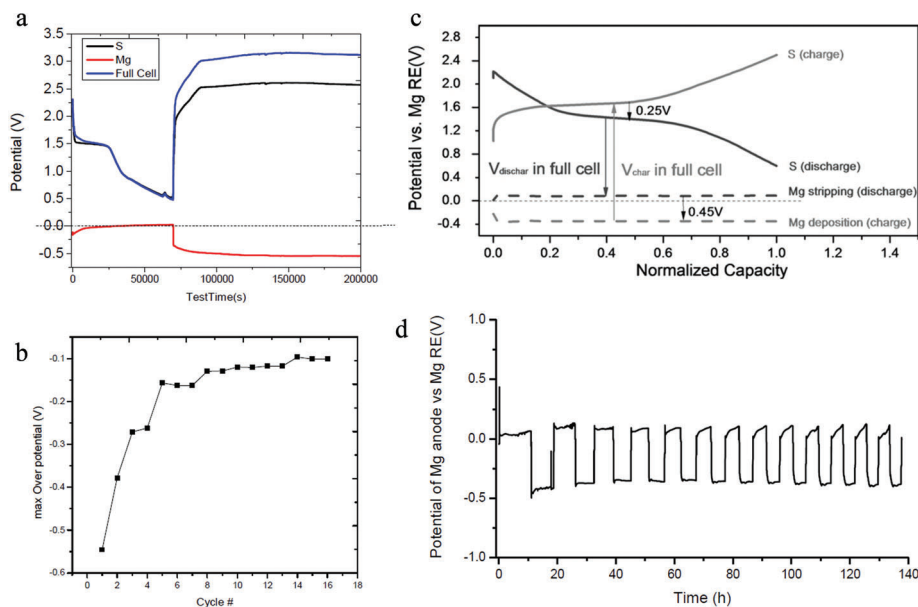
**ADVANCED
SCIENCE NEWS**

www.advancedsciencenews.com

**ADVANCED
ENERGY
MATERIALS**

www.advenergymat.de

Figure 13. Investigation of the overpotential evolution in three-electrode Mg–S cells. a) First cycle and b) ongoing cycling with 0.2 M MgHMDS + 0.5 M LiTFSI electrolyte. Reproduced with permission.[128] Copyright 2015, American Chemical Society. c) First cycle and d) Mg-anode potential in the ongoing cycles with 1 M MgTFSI + MgCl$_2$ in DME electrolyte. Reproduced with permission.[141] Copyright 2017, Wiley.

compromise in terms of capacity and conductivity is offered by SeS$_x$ compounds (x = 1–3)—with SeS$_2$ featuring the best electrochemical performance, that is, a small hysteresis and impressive capacity retention at 1C. However, its performance at room temperature is rather poor, indicating that the thermally activated Mg^{2+} diffusion still represents the bottle neck. Again, the most probable origin is the reduction and reoxidation of the crystalline product, with SeS$_2$ exhibiting the smallest overpotentials compared to Se and S in CV measurements. Thus, even cathodes with high SeS$_2$ loadings of 8 mg cm^{-2} show a fair capacity of 700 mAh g^{-1} at 0.2C (5.6 mA cm^{-2}).

4.1.3. Other Strategies to Enhance S/Se Redox Reactions

There are indeed approaches in Mg–S/Mg–Se research to tackle the slow cathode kinetics in the final reduction process applying either 1) polar solvents to enhance the poly-sulfide/selenide solubility, 2) redox mediators with catalytic effect, or 3) copper current collectors and additives contributing to the capacity gain.

The application of polar solvents with high donor number is beneficial for Mg-conversion cathodes as the solubility of polysulfides can be greatly enhanced utilizing more sulfur active material. Additionally, the S$_3^{\bullet-}$ radical would be stabilized in solution[142] enabling faster kinetics to the final product (**Figure 14**). A promising performance in terms of overpotentials, capacity gain, and cycling stability was recently reported applying DMSO[144]—however with a special anode-protected cell as polar solvents passivate bare Mg metal in direct contact. Despite reports on the development of protective layers (so called artificial SEI) of the Mg surface, which enable the use of carbonates as solvent,[147] there is no study which could proof a long-term cycling of Mg batteries with polar solvents like DMSO or DMF. Nevertheless, this research direction holds great promise to fundamentally alter the redox mechanism and the kinetics therein.

Another option is the application of redox mediators—either by host functionalization via heteroatom doping (N-doped carbon,[134] N-doped graphene,[132] and N and Co co-doped ZIF-C[148]) or by adding functional nanoparticles to the cathode (carbon black and TiN,[140] Co,[149,150] and VN[150]) and separator interlayer (TiS$_2$,[151] CNF,[152] rGO,[148] and Mo$_6$S$_8$[153]). However, the beneficial effect is rather small and vanishes with cycling,[140] due to abovementioned reorganization of sulfur species and blocking of reaction sites.

In recent years, the use of copper in Mg–S and Mg–Se cells has attracted attention—either as Cu current collectors,[154–157] Cu nanoparticles,[158,159] or Cu foam interlayer.[145] Recently, also Ni foam has been applied as current collector.[157] In all studies, the in situ formation of sulfides and selenides (Cu$_2$S/CuS, CuSe, or NiS) during cycling contributes to the capacity gain in the initial cycles. In subsequent cycles, the sulfides provide preferable adsorption sites for sulfur species, which mitigates their diffusion in the electrolyte. Furthermore, the use of nucleophilic electrolytes is enabled. Beside the chemical confinement of polysulfides, copper sulfides and selenides are also applied as sole active material CuS,[143,160–164] Cu$_3$S$_2$,[165] Cu$_9$S$_5$,[166] CuSe,[167] Cu$_{2-x}$Se,[168] Cu–Se@MC,[169] or CuS$_{1-x}$Se$_x$.[170] Therein, it is reported that the mechanism does not follow a classical conversion, but a displacement reaction between Mg^{2+} and Cu^{2+}.[161,162,168]

Applying additives, which function as both, redox mediator and active material might be indeed a promising approach to enhance the capacity gain and cycling stability. However, attention has to be paid to the attainable energy density as copper compounds, especially in case of macroscopic foam, introduces the cell weight and volume, at increased costs. Similar to cathodes with low sulfur loading, seemingly good results might be misleading and the concept might not hold considering realistic cell setups.[158]
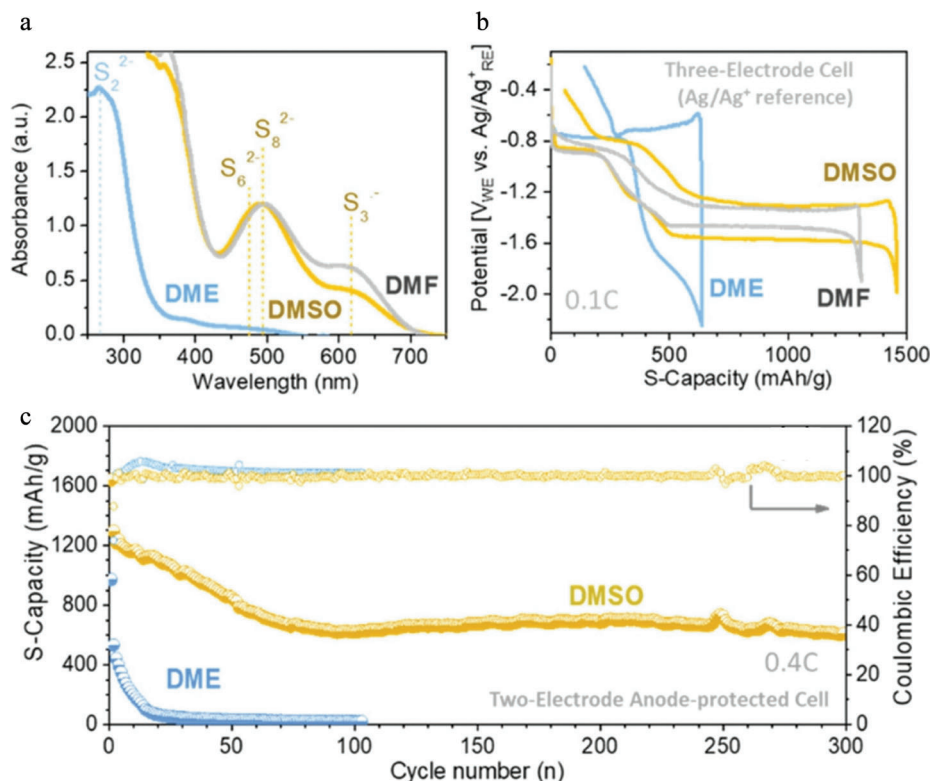
**ADVANCED
SCIENCE NEWS**

www.advancedsciencenews.com

**ADVANCED
ENERGY
MATERIALS**

www.advenergymat.de

Figure 14. Influence of the electrolyte solvent on the polysulfide solubility. a) UV–vis spectra of polysulfide solutions, b) discharge–charge cycle, and c) capacity retention of Mg–S cells applying non-polar (DME) and polar solvents (DMF and DMSO). Reproduced with permission.[144] Copyright 2021, Wiley.

Despite abovementioned approaches like uniform distribution of nanoparticles within a cathode host to shorten the diffusion path, polar solvents to stabilize crucial soluble intermediates or the introduction of redox mediators like cathode additives, current collectors, or separator interlayers to enhance the redox kinetics, the dissolution and diffusion of active material out of pores or even the cathode will lead to redistribution and partially inactive agglomerates. This emphasizes the intrinsic limitation of solid–liquid conversion materials (e.g., S, Se, and SeS_2)—namely the slow diffusion of Mg^{2+}—to finally become fatal for the cell performance.

4.1.4. Iodine Redox System

Similar as sulfur, iodine redox also undergoes a liquid–solid reaction pathway. In the presence of Mg^{2+}, I_2 is initially reduced to I_3^{2-} with the formation of an intermediate compound $Mg(I_3)_2$, which is highly soluble in ether-based electrolytes. However, its final discharge product MgI_2 is insoluble.[171] Compared with Mg–S batteries, Mg–I_2 batteries provide a higher voltage of 2.1 V and a lower capacity of 211 mAh g^{-1}, resulting in an energy density of >400 Wh kg^{-1}.[172] In addition to the cell voltage, another advantage of Mg–I_2 chemistry over Mg–S redox is the better compatibility with Mg metal anode. The presence of soluble iodide intermediates in the electrolyte allows reversible Mg plating/stripping rather than anode passivation, which is the case for Mg–S system. In fact, I_2 was applied as an electrolyte additive that

rendered extended cycle life in Mg–S batteries.[173] Overall, the Mg–I_2 chemistry offers favorable electrochemical kinetics. However, the formation of soluble intermediates leads to redistribution and agglomeration of the active species, which is detrimental for cycling stability as I_2 and iodides have low electronic conductivity. Furthermore, its dependence on the electrolyte amount needs further optimization strategies to control the soluble intermediate species.

4.2. Polymer Cathode with Flexible Molecular Structure

The abovementioned approaches rely on dissolution of intermediates and at least partial liquid phase conversion. To avoid the dissolution, active material redistribution, and polysulfide/selenide shuttle, a quasi-solid-state mechanism is proposed in Li–S batteries, which relies on the physical confinement in micropores and the formation of a CEI layer via electrolyte decomposition—commonly carbonates. As this approach is based on the solid-state diffusion of cations through the CEI or the carbon host, its utilization in Mg systems is precluded due to the insufficient solid-state diffusion. However, a solid–solid conversion is indeed achieved with covalently bound redox centers and redox-active polymers.

4.2.1. Covalently Bound S and Se

A popular approach to realize solid phase conversion in lithium batteries is the application of covalently bound
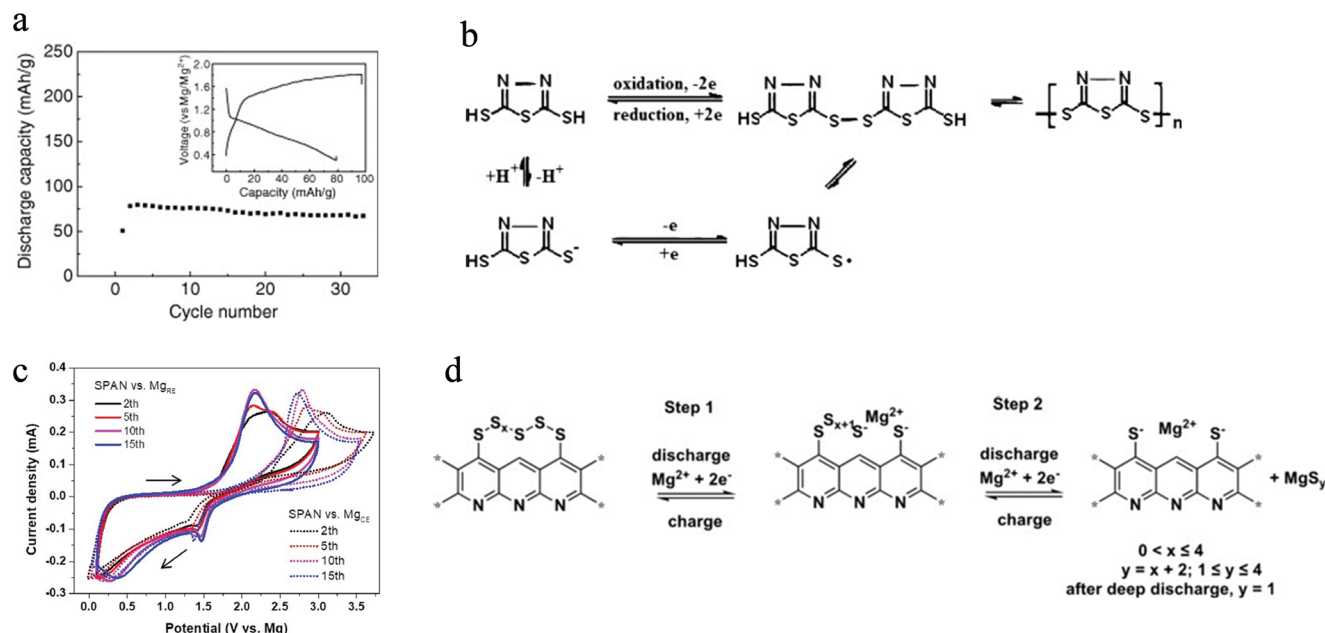
Figure 15. a) Galvanostatic cycling of a Mg–PDTDA cell. b) Proposed redox process for DMcT, Reproduced with permission.[174] Copyright 2007, Elsevier. c) CV of a Mg–SPAN cell applying 0.8 M $Mg[B(hfip)_4]_2$ in G2/G4 electrolyte with potential versus Mg–CE and Mg–RE and d) the proposed reduction and oxidation pathway therein. c) Reproduced with permission.[175] Copyright 2020, Elsevier. d) Reproduced according to the terms of the CC BY license.[178] Copyright 2020, The Authors, published by Wiley VCH.

sulfur in molecules or to a polymer backbone. To date, 2,5-dimercapto-1,3,4-thiadiazole (DMcT),[174] poly-2,20-dithiodianiline (PDTDA),[174] sulfurized poly(acrylonitrile) (SPAN),[156,174–179] and selenized poly(acrylonitrile) (SePAN)[180] have been investigated as potential cathode material in Mg–S and Mg–Se cells, respectively.

The redox pathway differs according to the applied polymer—exemplary proposed redox processes are illustrated in **Figure 15** for DMcT and SPAN with a stepwise reduction and oxidation of the S-chain covalently bound to the polymer backbone. This concept requires sufficient wetting of the active material with electrolyte to avoid a kinetic limitation due to solid state diffusion of Mg^{2+} ions. However, as depicted in Figure 15c, the solid conversion to the final product MgS is accompanied with large overpotentials. For this reason, hybrid electrolytes were applied in recent years to take advantage of the fast monovalent-ion diffusion to function as mediator and enhance the cathode kinetics (see Section 4.3.2).[176–180]

Note that despite such cathode concept, partially polysulfides are generated—as the anode shows some sulfur residues at its surface in post-mortem analysis.[175] Despite being beneficial for the kinetics, this results in active material loss and possible anode passivation. As the cycling stability nevertheless is greatly enhanced, this might also stem from elemental sulfur residues after active material synthesis.

4.2.2. Redox-Active Polymers/Organic Cathodes

Compared to the rigid and dense crystal structures of inorganic materials, organic compounds bounnded by weak intermolecular forces generally have loosely packed structures, providing energetically more favorable ionic pathways.[181] Particularly, the conjugated molecular structures allow easy charge delocalization that boosts the kinetics of the redox reactions enabling divalent Mg-ion storage at a higher current rate. Moreover, the merits of resource abundance and structural tunability add up to sustainability and electrochemical tailorability.

Organic materials have increasingly attracted attention as feasible cathode candidates for high-energy and high-power Mg batteries.[182,183] Quinone-based materials have been intensively studied. They are n-type compounds in which the carbonyl groups as the redox center undergo a reversible enolization reaction, offering a discharge voltage of >1.5 V versus Mg. Dimethoxybenzoquinone (DMBQ) was the first organic cathode probed in Mg battery systems using different electrolytes. By coupling with the electrolytes including $Mg(ClO_4)_2$ in γ-butyrolactone,[184] $Mg(BF_4)_2$ in EC/PC, $Mg(ClO_4)_2$ in PC, and $Mg(TFSI)_2$ in diglyme,[185] DMBQ cathode exhibited poor electrochemical performance in terms of low discharge voltage, large charge over-potential, and low reversibility mainly due to the unsatisfactory properties of the electrolytes. In contrast, the Mg cells with DMBQ cathode showed a flat voltage plateau at 2.0 V with an initial discharge of 226 mAh g^{-1} in the electrolyte $Mg(TFSI)_2$–$MgCl_2$ in DME.[185] However, rapid capacity fade was observed and a reversible capacity of 74 mAh g^{-1} was obtained after 30 cycles due to the high solubility of DMBQ and the inefficiency of the recharge.

The dissolution of organic molecules into the electrolyte is one of the general shortcomings of this type of electrode materials. Fortunately, it can be effectively circumvented by use of insoluble polymers. In addition, an appropriate selection of electrolyte generally represents a key for enabling reversible Mg batteries and plays a vital role in achieving high
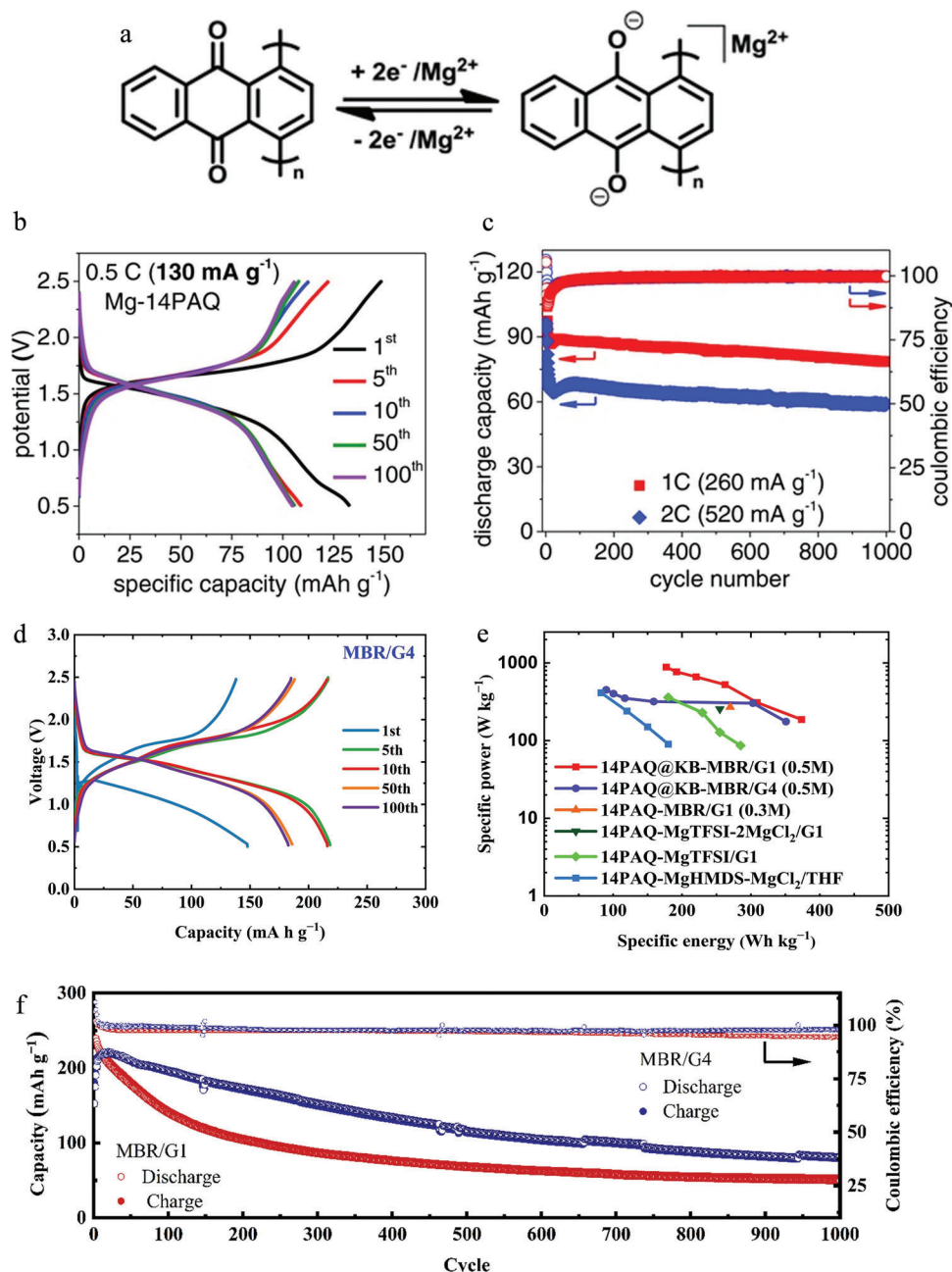
**ADVANCED
SCIENCE NEWS**

www.advancedsciencenews.com

**ADVANCED
ENERGY
MATERIALS**

www.advenergymat.de

Figure 16. a) Enolation redox reaction equation of 14PAQ. b) Galvanostatic discharge–charge curves and c) cycling performance of Mg–14PAQ cells with $Mg(HMDS)_2$–$MgCl_2$ electrolytes. Reproduced with permission.[187] Copyright 2016, Wiley. d) Discharge–charge profiles Mg–14PAQ cells with $Mg[B(hfip)_4]_2$ electrolytes in tetraglyme (G4). e) Ragone plots showing the performance of 14PAQ cathodes with different Mg electrolytes. f) Cycling performance of Mg–14PAQ cells in $Mg[B(hfip)_4]_2$ electrolytes in DME (G1) and tetraglyme (G4). Reproduced according to the terms of the CC BY license.[188] Copyright 2021, The Authors, published by Wiley VCH.

performance. A comparative study of poly(anthraquinonyl sulfide)-based cathodes with various electrolyte systems revealed that $Mg(TFSI)_2$–$MgCl_2$ electrolyte enabled better electrochemical performance (a reversible capacity of about 50 mAh g^{-1} after 100 cycles) compared to the systems with $Mg(HMDS)_2$–$AlCl_3$ or $MgCl_2$–$AlCl_3$ electrolytes.[121]

Poly-1,4-anthraquinone (P14AQ) has also been considered as a promising organic cathode for Mg batteries because it combines the features of a low LUMO energy level correlated to a high reduction potential and relatively high capacity based on the two-electron enolation reaction (**Figure 16**a).[186] The Mg–P14AQ system displays a discharge voltage of 1.6 V in $Mg(HMDS)_2$–$MgCl_2$ (HMDS: hexamethyldisilyzide) electrolyte and a long-cycling-life of 1000 cycles with 90% of capacity retention at a rate of 1C (Figure 16b,c).[187] While these chloro-complex-based systems have been the most employed electrolytes in Mg battery research

due to their electrochemical stability and ease of preparation, it has been revealed that the charge storage mechanism with the Cl-containing electrolytes involves MgCl$^+$ shuttling instead of divalent Mg^{2+} ions as charge carriers, which leads to a reduced energy density at cell level.[91]

In the past, substantial research efforts have been devoted to rational design of stable and efficient Mg electrolytes.[14] In particular, Cl-free non-corrosive magnesium tetrakis(hexafluoroisopropyloxy) borate (Mg[B(hfip)$_4$]$_2$)-based electrolytes possessing high oxidative stability (>4 V) and high ionic conductivity ($\approx$11 mS cm^{-1}) provide new prospects for the realization of high-performance Mg batteries.[99,189] By employing the Mg[B(hfip)$_4$]$_2$/tetraglyme (MBR/G4) electrolytes, the P14AQ composite-based cathodes (denoted as 14PAQ@KB) exhibited superior electrochemical performance in terms of rate capability, high-power, high-energy density, and long-term cycling stability (81 mA h g^{-1} after 1000 cycles) as shown in (Figure 16d–f).[188] This study indicates that the charge storage mechanism of organic cathodes upon de-/magnesiation differs with the used electrolytes and that optimizing the electrolyte–electrode combinations is crucial for achieving high-performance Mg batteries. Further, it has been reported that pyrene-4,5,9,10-tetraone with four carbonyl groups could reach a specific capacity of 315 mAh g^{-1} and a cell voltage of 2.1 V versus Mg with the boron cluster Mg(CB$_{11}$H$_{12}$)$_2$-based electrolytes.[9]

Recently, p-type organic materials have also been investigated for high-voltage and high-power Mg batteries. Magnesium-based dual ion batteries consisting of redox polymer (poly(vinyl carbazole) [PVCz]) cathodes and de-magnesiated alloy-type anodes (3Mg/Mg$_2$Sn) in Mg(TFSI)$_2$/ACN exhibit a cell voltage of $\approx$3 V and stable cycling properties with a capacity retention of 94.2% after 2000 cycles (see **Figure 17**a,b).[190] Another 3-V Mg system has been demonstrated with a polytriphenylamine (PTPAn) composite cathode and Mg metal anode in a Mg[B(hfip)$_4$]$_2$-based electrolyte.[191] Through the interaction between amine functional groups of the polymer cathode with the [B(hfip)$_4$] anions, reversible redox at the amine N center was achieved (Figure 17c). As a result, the PTPAn cathodes showed superior rate capability and a long-cycling performance at 10C (Figure 17d,e). The dual-ion Mg cells via an anion-storage mechanism provide a promising approach toward high-power density Mg batteries. It is worth mentioning that the energy density of dual-ion systems at cell level is generally limited by the requirement of a relatively large amount of electrolyte as both cation and anion act as charge carriers. Nevertheless, due to the two-electron transfer per Mg^{2+} ion and double mole ratio of the counter anions in the electrolytes, the amount of electrolyte for the divalent dual-ion systems might be substantially reduced, leading to improved energy density compared to the respective monovalent systems.

To summarize, organic cathodes with intrinsically favorable redox kinetics can be considered as promising candidates for high-energy Mg batteries. Recent studies indicate that a proper combination of cathode and electrolyte is crucial for achieving high-performance organic Mg batteries. The advancement in Mg electrolytes with favorable electrochemical properties is accelerating the development of Mg batteries with long cycle life and improved rate capability.

4.3. Hybrid Systems

Mg hybrid batteries refer to Daniell-type cells, where a cathode which is hosting monovalent charge carrier (such as Li$^+$ and Na$^+$) is coupled with a metallic Mg anode (see **Figure 18**a).[122] This concept requires a high Coulombic efficiency, that is, reversibility, as the monovalent ions only stem from the dual-salt electrolyte with no additional reservoir. Without physical separation of the carriers, the charge compensation for redox reactions at cathode is fulfilled by kinetically favorable monovalent cations while the anode processes are governed by thermodynamics in favor of Mg plating/stripping.[192] Therefore, the hybrid concept could potentially combine the fast kinetics and high energy efficiency of monovalent charge carriers with an energy-dense metal anode with high safety.

4.3.1. Hybrid Electrolyte with Insertion Cathode

As the cathode accommodates monovalent ions, host structures developed for LIBs or SIBs were intensively investigated. In addition to the abovementioned advantages, the high-voltage cathodes add more practical value to the energy storage system especially when it comes to cell or pack level. As a proof-of-concept, Yagi et al. demonstrated a Mg–Li hybrid cell with a LiFePO$_4$ cathode, which delivered an initial capacity of 120 mAh g^{-1} at 2.5 V versus Mg.[122] The cycling performance of the system was largely improved by employing a graphite foil current collector, which is more stable against the Cl-based electrolyte.[194] Interestingly, the Mg–Li system exhibited superior battery performance over pure Li system at low temperature, highlighting its potential application scenario. With the development of Mg electrolyte, other host structures including layered oxide and spinel oxide that provide redox reactions at higher voltages were studied.[195] The LiMn$_2$O$_4$ spinel cathode was cycled against Mg anode in a Mg(TFSI)$_2$–LiTFSI electrolyte, showing a cell voltage of 2.8 V at 0.2C. Further optimization of cathode structure and its compatibility with electrolyte might result in a 3 V class Mg metal cell.

Compared to Mg–Li hybrid systems, Mg–Na hybrid cells can be more sustainable and cost effective, and promising for large-scale application. To this end, a Prussian blue analogue Na$_x$Fe$_2$(CN)$_6$ was reported in a hybrid cell configuration.[196] The Berlin green cathode delivered a reversible capacity of 143 mAh g^{-1} at an average voltage of 2.2 V versus Mg. When considering the total weight of cathode, electrolyte (Na reservoir) and anode, the cell provided a specific energy of 135 Wh kg^{-1} and could be cycled up to a specific power of 1.67 kW kg^{-1}. Inspired by this work, further investigation on a Na$_3$V$_2$(PO$_4$)$_3$ cathode showcased a Mg–Na hybrid system, which exhibited an average cell voltage of 2.6 V with a capacity of 100 mAh g^{-1}.[197] Benefiting from the excellent Na-ion mobility in the NASICON-type structure, fast charging of the cell was demonstrated with 86% capacity retention at 10C. Beyond the NASICON structures, a higher specific energy of 183 Wh kg^{-1} (based on cathode with theoretical amount of electrolyte and anode) can be reached by applying a NaCrO$_2$ cathode.[198] At a cell level, the Mg-based hybrid system shows the potential to reach 100 Wh kg^{-1},[199] which can be attractive for grid storage. And this calls for further detailed
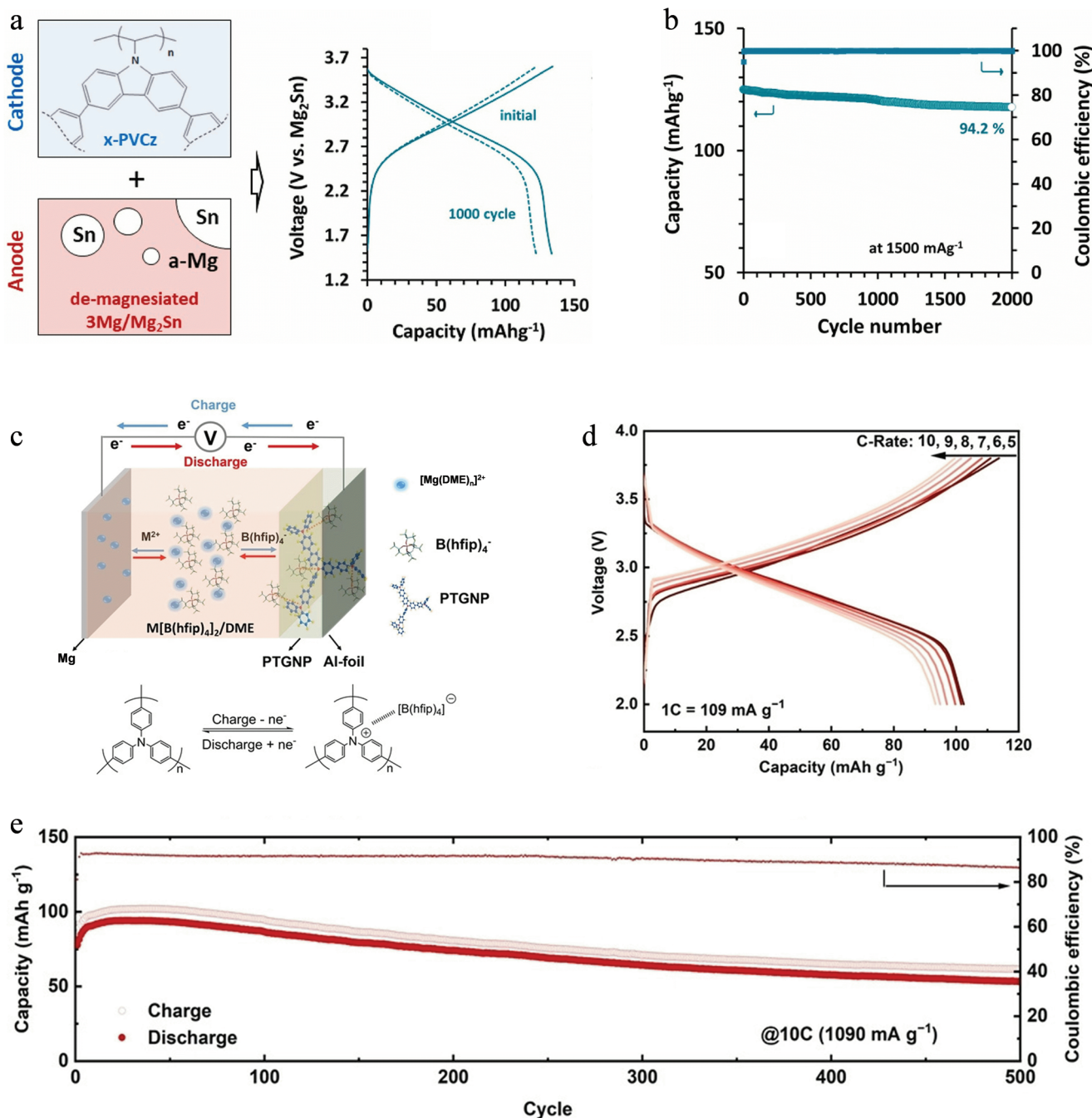
Figure 17. PVCz∥3Mg/Mg₂Sn dual-ion cell: a) scheme of the cell configuration and discharge/charge profiles and b) cycling performance. Reproduced with permission.[190] Copyright 2021, Elsevier. Mg∥PTPAn cell with Mg[B(hfip)₄]₂/DME electrolyte: c) cell configuration and the working principle, d) galvanostatic voltage profiles at various C-rates (i.e., 5–10C), and e) cycling performance at 10C. Reproduced according to the terms of the CC BY license.[191] Copyright 2022, The Authors, published by Wiley VCH.

investigation in more realistic test conditions to validate the practicality of the concept.

Note that by applying dual-salt electrolyte, another scenario apply, where both charge carriers are shuttling between cathode and anode. As shown in Figure 18b, this results in a rocking-chair type battery. Such configuration does not require excess amount of electrolyte as carrier ion reservoir, and thereby being promising to achieve a higher energy density than the Daniell-type battery. The concept was brought by Ichitsubo et al. employing a high-voltage $MgCo_2O_4$ spinel cathode with a $Mg_{49}Li_{51}$ alloy anode.[200] Due to the co-storage of Mg and Li, the cathode capacity amounted to 150–200 mAh g⁻¹ at an average cell voltage of 2.5 V (yet tested at an elevated temperature of 150 °C).
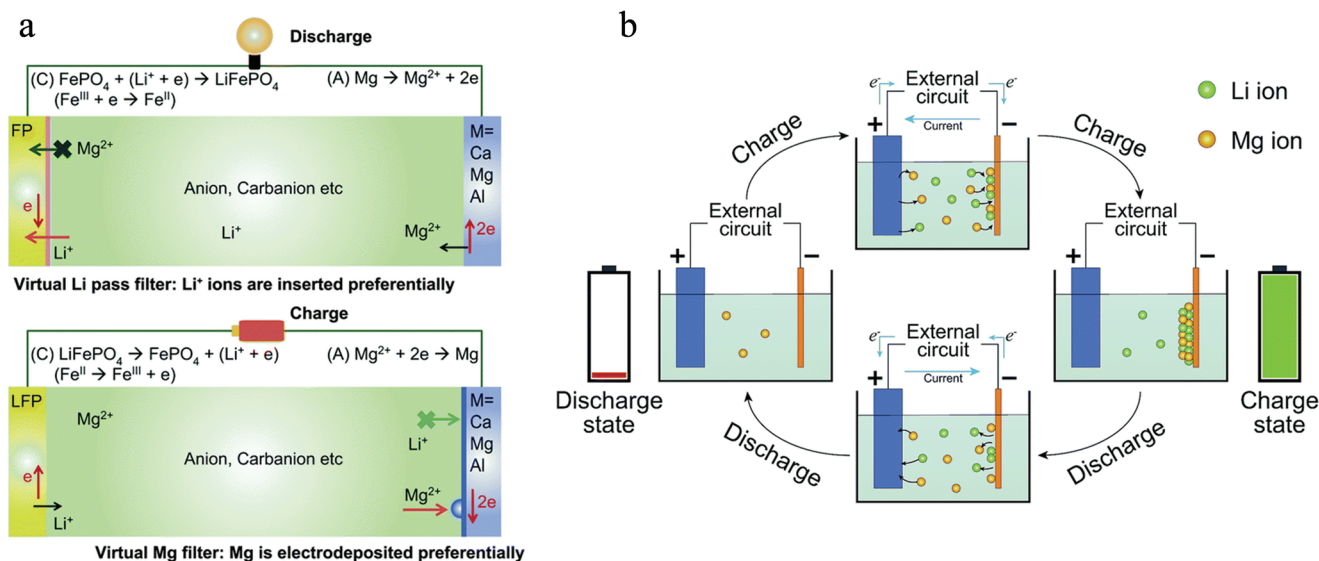
**ADVANCED
SCIENCE NEWS**

www.advancedsciencenews.com

**ADVANCED
ENERGY
MATERIALS**

www.advenergymat.de

Figure 18. a) Schematics of the Daniell-type Mg-based hybrid cell. Reproduced with permission.[122] Copyright 2013, The Royal Society of Chemistry. b) Schematics of rocking-chair type dual-salt battery. Reproduced with permission.[193] Copyright 2017, The Royal Society of Chemistry.

To validate the feasibility of the rocking-chair type dual salt battery at room temperature, Chevrel phase Mo_6S_8 with high Mg-ion conductivity was introduced. Elemental analysis of the cycled electrodes revealed a cooperative insertion of both charge carriers, with Li^+ initially occupying the energetically less favorable sites followed by a co-insertion until full occupation.[193] Based on further theoretical investigation, a concerted motion mechanism was proposed where the Mg^{2+} mobility was enhanced by the "push" of the neighboring Li^+.[201] Despite a high degree of co-insertion (up to $Li_{1.27}Mg_{1.27}Mo_6S_8$) observed in Mo_6S_8, Mg content in other co-inserted cathodes was still limited.[202,203] It seems that the intrinsic mobility of Mg is still decisive, which however might be improved if the assisting monovalent charge carrier was able to optimize the diffusion pathway such as coordination environment.

4.3.2. Mg–S Batteries with Dual-Salt Electrolyte

Adding Li salts to the Mg electrolyte to enhance the cathode conversion kinetics was first investigated in 2015 by Gao et al. in Mg–S cells using LiTFSI[128] and has become popular in recent years by incorporating LiTFSI,[148] LiCl,[179,204,205] LiBr,[206] $LiCF_3SO_3$,[176,205] $Li[B(hfip)_4]$,[207] and $Li[BH_4]$.[178] In such hybrid systems, Li^+ serves as mediator to result in lower overpotentials, higher capacity gain, and reduced capacity fading. Regarding the cathode side, different origins are proposed,[128] wherein the hard Lewis acid Li^+ plays an active role in dissolving MgS by 1) strongly coordinating to the surface S^{2-} of MgS and increasing its solubility,[176,208] 2) lithiating MgS due to the natural negative potential of Mg metal, forming soluble higher order MgLi-PS,[209] and/or 3) an ion exchange reaction (MgS to Li_2S).

The proposed pathway differs for elemental and covalently bound sulfur cathodes (**Figure 19**). Taking SPAN as an example, long-chain polysulfides (i.e., MgS_8) are not formed due to

the strong S–C bond and sulfur chain length restrictions within the molecule.[176] Yet in both cases, the kinetics are significantly enhanced resulting in lower voltage hysteresis and better sulfur utilization. This becomes obvious by the fact, that the conversion kinetics are mainly diffusion-controlled (cf. Figure 10e,f)[176] and the diffusion of Li^+ is superior to the high-charge dense Mg^{2+} cation. In addition, the Li additive contributes to the formation of an ion-conductive CEI layer consisting of SO_x^{2-}.[179]

A clear advantage of such approach is the use of sulfur cathodes developed for the Li–S system like tailored carbon hosts (e.g., sulfide graphdiyne),[204] metal–organic frameworks,[148] or sulfurized polymers (SPAN[176,178] or SePAN[180]) (**Figure 20**), which rely on the solid-state diffusion of Li^+ ions and would otherwise be mostly excluded for the use in Mg–S batteries.[204] Furthermore, the application of carbonate-based or nucleophilic electrolytes like APC is enabled[204] and the use of polymeric membranes instead of glass fiber separators is possible,[179] which is essential to realize high-energy Mg–S batteries.

To achieve this meditation effect and incorporate Li^+ in the sulfur redox reaction pathway, a rather high concentration of Li salt is necessary—thus speaking of an additive is inappropriate (**Figure 21**a).[178] Interestingly, a too high concentration can be in fact also detrimental due to transport limitations (diffusivity and conductivity).[205] Furthermore, as there is no Li source within the cell, full reversibility has to be secured, which remains questionable. However, as neither Li deposition nor Li–Mg alloying was observed in XRD and XPS analysis on the Mg anode,[128] Mg is the only active species during stripping/plating at the anode, which might be additionally enhanced by the presence of a Li salt.[210] Note, that a larger surface area of the Mg anode is also beneficial to reduce the local current density and overpotentials, and increases the capacity gain (Figure 21b).[178] Such hybrid electrolyte might therefore be indeed a promising approach to combine fast sulfur cathode kinetics with a dendrite-free Mg anode.
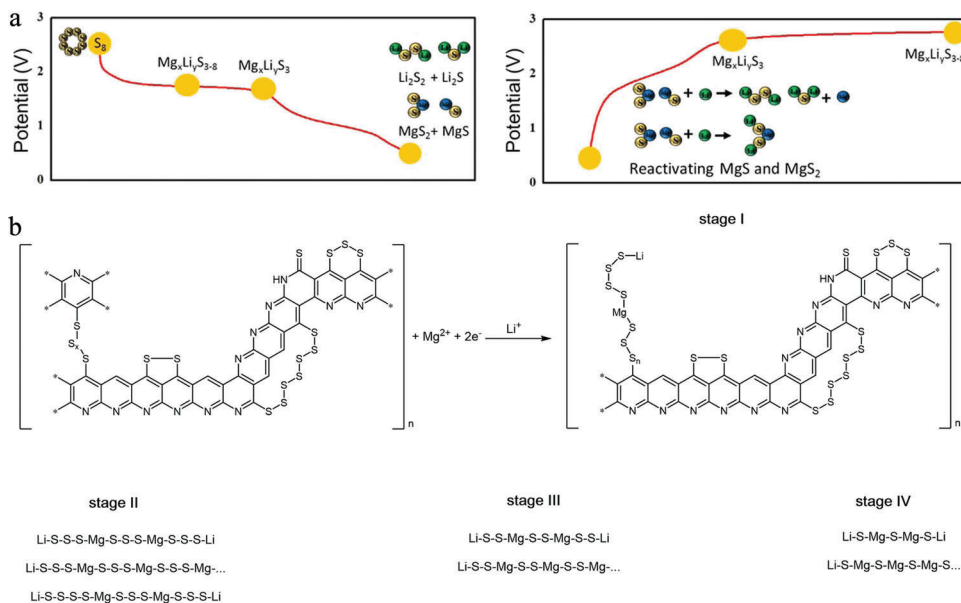
Figure 19. Proposed schematic pathway of a Mg–S cell with a) ACC/S cathode and LiTFSI electrolyte additive and b) SPAN-cathode and Li triflate electrolyte additive. a) Reproduced with permission.[128] Copyright 2015, American Chemical Society. b) Reproduced with permission.[176] Copyright 2021, Elsevier.
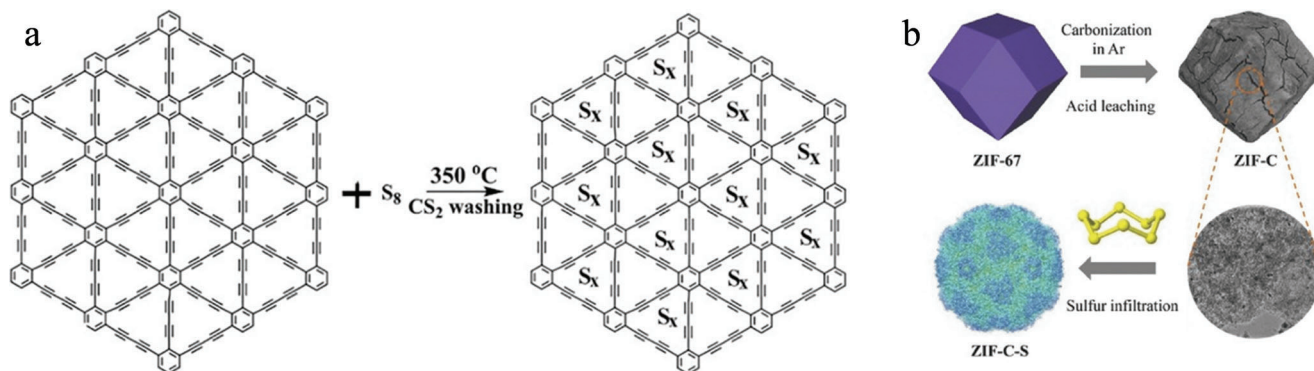

Figure 20. a) Sulfide graphdiyne (SGDY) featuring high Li$^+$ mobility and short-chain sulfur species. Reproduced with permission.[204] Copyright 2017, Wiley. b) S-loaded metal–organic framework ZIF-C. Reproduced with permission.[148] Copyright 2018, Wiley.

5. Perspectives

The successful commercialization and wide application of LIBs demonstrated the technical advantages of rechargeable ion batteries as efficient energy storage system, but also arouse enormous interest to research on other chemistries beyond Li-ion. While post-Li systems may hardly provide higher battery performance, they could be competitive in terms of sustainability, cost and environmental impact. In fact, these criteria are becoming more relevant so as to lower the carbon footprint as fast as possible by promoting large-scale applications. However, there is still a long way to go before the merits of post-lithium batteries in practical scenario can be achieved.

Kinetic hindrance is one of the critical roadblocks for divalent systems. This issue is a result of strong interaction between the highly polarizing charge carrier and the host lattice. Worse is that the ion–dipole interaction sometimes even triggers conver-sion reaction as the thermodynamically favorable process over intercalation,[31] which makes the Mg^{2+}-based chemistry more complicated. To tackle the intrinsic limitations of the divalent carriers, unconventional approaches with respect to those applied in monovalent ion storage have been proven more feasible to unlock the kinetic limitations, leading to progressive understanding of the charge/ion storage principle and its impact on the host structural stability. As multivalent-ion batteries share some general chemistries, lessons can also be learned from the feasible strategies developed for the systems with other multivalent cations, such as Zn^{2+}, Ca^{2+}, and Al^{3+}.

To weaken the Mg–cathode interaction is unambiguously the primary goal for the development of viable host structures. Improved Mg mobility is evident either in a softer lattice or through an energetically favorable diffusion pathway. The former implies a decisive role of the electronic structures governed by the orbital energy of individual atoms that form the crystal
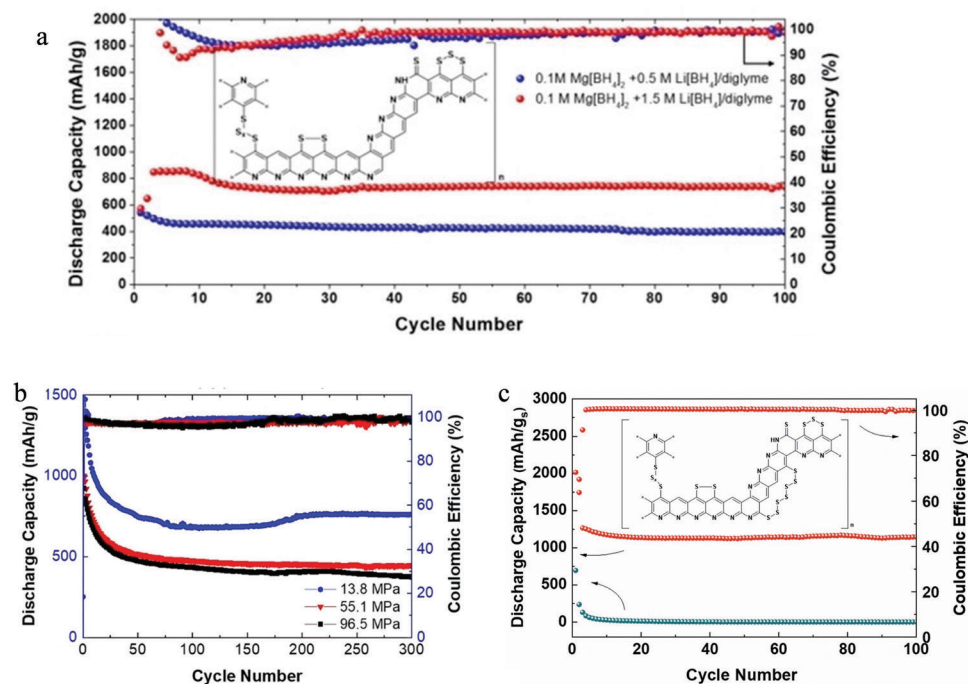
**ADVANCED
SCIENCE NEWS**

www.advancedsciencenews.com

**ADVANCED
ENERGY
MATERIALS**

www.advenergymat.de

Figure 21. Mg–SPAN cells with a) liquid electrolyte based on Mg[BH₄]₂ and Li[BH₄], and b) Mg powder anodes prepared at different pressures. Reproduced according to the terms of the CC BY license.[178] Copyright 2020, The Authors, published by Wiley VCH. c) The highest and most stable reported capacity of Mg–S cells after 100 cycles to date. Reproduced with permission.[176] Copyright 2021, Elsevier.

unit. Delocalization of outer electrons in the cluster unit can effectively screen the double charge of Mg-ions, but also offer flexible multielectron transfer for easy local charge balancing.[43] This normally triggers multiple redox centers including ligands in addition to TM atoms, which however may destabilize the lattice structure under repeated electronic attack.[68] Therefore, a desired electronic structure should provide an optimized charge allocation on each redox center to extend the cycling stability.

The crystal structure also affects the energy profile for Mg^{2+} diffusion. However, as the lattice is much more sensitive upon Mg^{2+} uptake, most of the geometries reported provide diffusion energy penalties beyond the realistic thresholds. Nevertheless, some of them such as layered structures and open frameworks (mainly Prussian blue analogues[211] and NASICON materials) exhibit highly structural tunability. While in layered materials, the diffusion channels can be expanded to a large extent, rendering sufficient ionic mobility, the open framework structures of NASICON-type compounds are made of polyanion tetrahedras and metal oxide octahedras by corner sharing, offering structural variety by allowing different connections between the polyhedras.[212] In fact, NASICON families are known to be super ionic conductors. Via a proper design of their TM redox and coordination environment, these materials have the potential to provide high voltage and high energy density in Mg systems.[213] Another promising crystal engineering strategy is to introduce dopants that create defects as additional Mg percolation pathways. The outstanding performance of vacancy-doped anatase TiO_2 demonstrated the feasibility to construct diffusion highways for multivalent carriers by defect chemistry.[60]

Alternatively, replacing Mg^{2+} by other Mg-based carriers with lower charge density reduces the Coulombic interaction with the host structure, resulting in improved diffusion kinetics.[22,85] The incorporation of additional anions or solvent molecules leads to the formation of ternary intercalation compounds, by which the thermodynamics as well as kinetics can be adjusted. As Mg^{2+} tends to form either strong solvation shells or ion pairs in the electrolyte, new insertion chemistries with Mg-based carriers can be designed. To trigger the redox reaction, capability of the cathode materials with respect to reversibly hosting larger cations should be considered. This can be achieved by the abovementioned crystal engineering strategies or design a flexible solvation structure for easy Mg^{2+} insertion (e.g., with a low reorganization energy[20]). In addition, practical evaluation should be carried out carefully by taking into account the amount of electrolyte that serves as the reservoir for the co-inserted solvents or anions.

The success of cointercalation strategies to improve the kinetics also reflects the interfacial issue, as it circumvents the desolvation process at the cathode–electrolyte interface. In fact, the large desolvation energy barrier could also explain the controversial findings regarding Mg^{2+} storage capability in some cathode materials with different electrolytes. While the coordination strength of Mg^{2+} in the electrolyte is much higher than that of Li^+, interfacial processes should be treated equally important as solid diffusion. More efforts on this topic would clarify the kinetic limit, so that Mg^{2+} storage and diffusion in solids can be better understood. To promote interfacial charge/ion transfer, cathode–electrolyte compatibility should be optimized. This calls for further development of electrolyte that provides weaker solvation environments for Mg^{2+}, or forms stable solid interphases for energetically favorable transfer processes.

Beyond intercalation, electrochemistries that (partially) bypass the solid diffusion processes are kinetically favorable for Mg sys-

tems. These strategies mainly involve (quasi) interfacial redox reactions, by triggering heterogeneous redox reactions or applying flexible molecular chain-like structures. In both cases, the cathode materials rely on more abundant elements by getting rid of TMs, thereby being more sustainable yet with low conductivity. As a result, conductive matrices with high surface area are beneficial for fast charge transfer and/or more redox active sites. A challenge for small molecular materials (both organic and S-based compounds) is their solubility in the electrolyte, leading to the loss of active materials. Dissolution of these materials or their reaction intermediates can be suppressed via enhancement of the conversion kinetics, by, for example, structural modification, addition of redox mediators, or introducing 3D hierarchical substrate with strong affinity to the specific active material. As redistribution of active materials can be hardly avoided, other strategies like anode protection or separator modification should be implemented for better reversibility. Polymerization is a promising strategy to ultimately solve the dissolution issue. Polymer cathodes provide flexible backbones that hold the redox active moieties through chemical bonding, and meanwhile allow easy access of electrolyte. Although this type of material delivered the best cycling performance in Mg batteries, further efforts are needed to increase the mass loading as well as the content of active materials for achieving high energy density.

In addition, hybrid Mg batteries hold the promise to combine fast-kinetic monovalent cathode chemistry and high-capacity metal anodes, which deserves further evaluation under practical aspects. To have an even more sustainable and cost-effective approach, Na^+ or K^+ can be applied instead of Li^+ ions. Based on the well-developed materials in monovalent systems, high-voltage or high-capacity cathodes with high loading can be employed. A rough evaluation of such systems based on the transfer rate of LIBs indicates that an energy density of 100 Wh kg^{-1} may be reached at cell level, which could be considered for stationary applications. Challenges of such systems are largely associated with the electrolyte, as to whether it has good compatibility with high-voltage cathode, but also to lower the electrolyte to cathode ratio. The latter is more critical for achieving high energy density.

Overall, the development of cathode chemistries for Mg batteries is still at low technology readiness levels. The key challenges are not only the kinetic limitations of bulk Mg^{2+} diffusion, but also combinatory issues of other transport processes. In a lot of cases, the gained capacity depends on the applied electrolyte, which calls for careful evaluation by a proper selection of cathode–electrolyte combination or even considering the whole charging loop of the full-cell. Based on that, strategies with synergetic effect may ultimately lead to a breakthrough of the cell performance that pushes the Mg technology one-step forward.

Acknowledgements

Conflict of Interest

The authors declare no conflict of interest.

Keywords

[1] Z. P. Cano, D. Banham, S. Ye, A. Hintennach, J. Lu, M. Fowler, Z. Chen, *Nat. Energy* **2018**, *3*, 279.
[2] A. Manthiram, *ACS Cent. Sci.* **2017**, *3*, 1063.
[3] V. Viswanathan, A. H. Epstein, Y.-M. Chiang, E. Takeuchi, M. Bradley, J. Langford, M. Winter, *Nature* **2022**, *601*, 519.
[4] IMA Europe, Recycling Industrial Minerals **2018**.
[5] P. Bai, J. Li, F. R. Brushett, M. Z. Bazant, *Energy Environ. Sci.* **2016**, *9*, 3221.
[6] S. Dühnen, J. Betz, M. Kolek, R. Schmuch, M. Winter, T. Placke, *Small Methods* **2020**, *4*, 2000039.
[7] D. Aurbach, Z. Lu, A. Schechter, Y. Gofer, H. Gizbar, R. Turgeman, Y. Cohen, M. Moshkovich, E. Levi, *Nature* **2000**, *407*, 724.
[8] M. Jäckle, K. Helmbrecht, M. Smits, D. Stottmeister, A. Groß, *Energy Environ. Sci.* **2018**, *11*, 3400.
[9] H. Dong, O. Tutusaus, Y. Liang, Y. Zhang, Z. Lebens-Higgins, W. Yang, R. Mohtadi, Y. Yao, *Nat. Energy* **2020**, *5*, 1043.
[10] G. A. Elia, K. Marquardt, K. Hoeppner, S. Fantini, R. Lin, E. Knipping, W. Peters, J.-F. Drillet, S. Passerini, R. Hahn, *Adv. Mater.* **2016**, *28*, 7564.
[11] Y. Tian, G. Zeng, A. Rutt, T. Shi, H. Kim, J. Wang, J. Koettgen, Y. Sun, B. Ouyang, T. Chen, Z. Lun, Z. Rong, K. Persson, G. Ceder, *Chem. Rev.* **2021**, *121*, 1623.
[12] Y. Liang, H. Dong, D. Aurbach, Y. Yao, *Nat. Energy* **2020**, *5*, 646.
[13] P. Canepa, G. S. Gautam, D. C. Hannah, R. Malik, M. Liu, K. G. Gallagher, K. A. Persson, G. Ceder, *Chem. Rev.* **2017**, *117*, 4287.
[14] R. Mohtadi, O. Tutusaus, T. S. Arthur, Z. Zhao-Karger, M. Fichtner, *Joule* **2021**, *5*, 581.
[15] R. Deivanayagam, B. J. Ingram, R. Shahbazian-Yassar, *Energy Storage Mater.* **2019**, *21*, 136.
[16] Z. Ma, D. R. MacFarlane, M. Kar, *Batteries Supercaps* **2019**, *2*, 115.
[17] R. Attias, M. Salama, B. Hirsch, Y. Goffer, D. Aurbach, *Joule* **2019**, *3*, 27.
[18] M. Mao, T. Gao, S. Hou, C. Wang, *Chem. Soc. Rev.* **2018**, *47*, 8804.
[19] C. Chen, F. Shi, Z.-L. Xu, *J. Mater. Chem. A* **2021**, *9*, 11908.
[20] S. Hou, X. Ji, K. Gaskell, P.-F. Wang, L. Wang, J. Xu, R. Sun, O. Borodin, C. Wang, *Science* **2021**, *374*, 172.
[21] S. H. Lapidus, N. N. Rajput, X. Qu, K. W. Chapman, K. A. Persson, P. J. Chupas, *Phys. Chem. Chem. Phys.* **2014**, *16*, 21941.
[22] H. D. Yoo, Y. Liang, H. Dong, J. Lin, H. Wang, Y. Liu, L. Ma, T. Wu, Y. Li, Q. Ru, Y. Jing, Q. An, W. Zhou, J. Guo, J. Lu, S. T. Pantelides, X. Qian, Y. Yao, *Nat. Commun.* **2017**, *8*, 339.
[23] J. Zhang, Z. Chang, Z. Zhang, A. Du, S. Dong, Z. Li, G. Li, G. Cui, *ACS Nano* **2021**, *15*, 15594.
[24] J. Bitenc, A. Scafuri, K. Pirnat, M. Lozinšek, I. Jerman, J. Grdadolnik, B. Fraisse, R. Berthelot, L. Stievano, R. Dominko, *Batteries Supercaps* **2021**, *4*, 214.
[25] J. Asenbauer, T. Eisenmann, M. Kuenzel, A. Kazzazi, Z. Chen, D. Bresser, *Sustainable Energy Fuels* **2020**, *4*, 5387.
[26] R. Shannon, *Acta Crystallogr. A* **1976**, *32*, 751.

[27] R. Zhang, T. S. Arthur, C. Ling, F. Mizuno, *J. Power Sources* **2015**, *282*, 630.

[28] G. S. Gautam, P. Canepa, A. Abdellahi, A. Urban, R. Malik, G. Ceder, *Chem. Mater.* **2015**, *27*, 3733.

[29] D. A. Kitchaev, S. T. Dacek, W. Sun, G. Ceder, *J. Am. Chem. Soc.* **2017**, *139*, 2672.

[30] R. Zhang, X. Yu, K.-W. Nam, C. Ling, T. S. Arthur, W. Song, A. M. Knapp, S. N. Ehrlich, X.-Q. Yang, M. Matsui, *Electrochem. Commun.* **2012**, *23*, 110.

[31] C. Ling, R. Zhang, T. S. Arthur, F. Mizuno, *Chem. Mater.* **2015**, *27*, 5799.

[32] S. Rasul, S. Suzuki, S. Yamaguchi, M. Miyayama, *Electrochim. Acta* **2013**, *110*, 247.

[33] T. S. Arthur, R. Zhang, C. Ling, P.-A. Glans, X. Fan, J. Guo, F. Mizuno, *ACS Appl. Mater. Interfaces* **2014**, *6*, 7004.

[34] H. D. Yoo, J. R. Jokisaari, Y.-S. Yu, B. J. Kwon, L. Hu, S. Kim, S.-D. Han, M. Lopez, S. H. Lapidus, G. M. Nolis, B. J. Ingram, I. Bolotin, S. Ahmed, R. F. Klie, J. T. Vaughey, T. T. Fister, J. Cabana, *ACS Energy Lett.* **2019**, *4*, 1528.

[35] P. Millet, C. Satto, P. Sciau, J. Galy, *J. Solid State Chem.* **1998**, *136*, 56.

[36] A. Mukherjee, N. Sa, P. J. Phillips, A. Burrell, J. Vaughey, R. F. Klie, *Chem. Mater.* **2017**, *29*, 2218.

[37] M. S. Whittingham, C. Siu, J. Ding, *Acc. Chem. Res.* **2018**, *51*, 258.

[38] J. L. Andrews, A. Mukherjee, H. D. Yoo, A. Parija, P. M. Marley, S. Fakra, D. Prendergast, J. Cabana, R. F. Klie, S. Banerjee, *Chem* **2018**, *4*, 564.

[39] M. Kar, O. Tutusaus, D. R. MacFarlane, R. Mohtadi, *Energy Environ. Sci.* **2019**, *12*, 566.

[40] R. Attias, M. Salama, B. Hirsch, Y. Gofer, D. Aurbach, *ChemElectroChem* **2018**, *5*, 3514.

[41] Z. Rong, R. Malik, P. Canepa, G. S. Gautam, M. Liu, A. Jain, K. Persson, G. Ceder, *Chem. Mater.* **2015**, *27*, 6016.

[42] M. Mao, X. Ji, S. Hou, T. Gao, F. Wang, L. Chen, X. Fan, J. Chen, J. Ma, C. Wang, *Chem. Mater.* **2019**, *31*, 3183.

[43] Y. Gu, Y. Katsura, T. Yoshino, H. Takagi, K. Taniguchi, *Sci. Rep.* **2015**, *5*, 12486.

[44] S. E. Cheon, C. W. Kwon, D. B. Kim, S. J. Hong, H. T. Kim, S. W. Kim, *Electrochim. Acta* **2000**, *46*, 599.

[45] X. Sun, P. Bonnick, V. Duffort, M. Liu, Z. Rong, K. A. Persson, G. Ceder, L. F. Nazar, *Energy Environ. Sci.* **2016**, *9*, 2273.

[46] I. Brown, *Acta Crystallogr. B* **1988**, *44*, 545.

[47] R. Zhang, C. Ling, *ACS Appl. Mater. Interfaces* **2016**, *8*, 18018.

[48] M. M. Thackeray, W. I. F. David, P. G. Bruce, J. B. Goodenough, *Mater. Res. Bull.* **1983**, *18*, 461.

[49] M. Liu, Z. Rong, R. Malik, P. Canepa, A. Jain, G. Ceder, K. A. Persson, *Energy Environ. Sci.* **2015**, *8*, 964.

[50] S. Okamoto, T. Ichitsubo, T. Kawaguchi, Y. Kumagai, F. Oba, S. Yagi, K. Shimokawa, N. Goto, T. Doi, E. Matsubara, *Adv. Sci.* **2015**, *2*, 1500072.

[51] K. Shimokawa, T. Atsumi, N. L. Okamoto, T. Kawaguchi, S. Imashuku, K. Wagatsuma, M. Nakayama, K. Kanamura, T. Ichitsubo, *Adv. Mater.* **2021**, *33*, 2007539.

[52] Q. D. Truong, H. Kobayashi, I. Honma, *RSC Adv.* **2019**, *9*, 36717.

[53] M. Liu, A. Jain, Z. Rong, X. Qu, P. Canepa, R. Malik, G. Ceder, K. A. Persson, *Energy Environ. Sci.* **2016**, *9*, 3201.

[54] X. Sun, P. Bonnick, L. F. Nazar, *ACS Energy Lett.* **2016**, *1*, 297.

[55] A. Emly, A. Van der Ven, *Inorg. Chem.* **2015**, *54*, 4394.

[56] P. Bonnick, X. Sun, K.-C. Lau, C. Liao, L. F. Nazar, *J. Phys. Chem. Lett.* **2017**, *8*, 2253.

[57] P. Lightfoot, F. Krok, J. L. Nowinski, P. G. Bruce, *J. Mater. Chem.* **1992**, *2*, 139.

[58] Y. Liang, H. D. Yoo, Y. Li, J. Shuai, H. A. Calderon, F. C. R. Hernandez, L. C. Grabow, Y. Yao, *Nano Lett.* **2015**, *15*, 2194.

[59] D. L. Duong, S. J. Yun, Y. H. Lee, *ACS Nano* **2017**, *11*, 11803.

[60] T. Koketsu, J. Ma, B. J. Morgan, M. Body, C. Legein, W. Dachraoui, M. Giannini, A. Demortière, L. Salanne, F. Dardoize, H. Groult, O. J. Borkiewicz, K. W. Chapman, P. Strasser, D. Dambournet, *Nat. Mater.* **2017**, *16*, 1142.

[61] C. Pei, Y. Yin, R. Sun, F. Xiong, X. Liao, H. Tang, S. Tan, Y. Zhao, Q. An, L. Mai, *ACS Appl. Mater. Interfaces* **2019**, *11*, 31954.

[62] S. D. Perera, R. B. Archer, C. A. Damin, R. Mendoza-Cruz, C. P. Rhodes, *J. Power Sources* **2017**, *343*, 580.

[63] L. Zhou, Q. Liu, Z. Zhang, K. Zhang, F. Xiong, S. Tan, Q. An, Y.-M. Kang, Z. Zhou, L. Mai, *Adv. Mater.* **2018**, *30*, 1801984.

[64] M. Lopez, H. D. Yoo, L. Hu, J. L. Andrews, S. Banerjee, J. Cabana, *ACS Energy Lett.* **2020**, *5*, 3357.

[65] W. Wang, Y. Jiang, Y. Yang, F. Xiong, S. Zhu, J. Wang, L. Du, J. Chen, L. Cui, J. Xie, Q. An, L. Mai, *ACS Nano* **2022**, *16*, 17097.

[66] J. Lee, A. Urban, X. Li, D. Su, G. Hautier, G. Ceder, *Science* **2014**, *343*, 519.

[67] Y. Wang, X. Xue, P. Liu, C. Wang, X. Yi, Y. Hu, L. Ma, G. Zhu, R. Chen, T. Chen, J. Ma, J. Liu, Z. Jin, *ACS Nano* **2018**, *12*, 12492.

[68] Z. Li, B. P. Vinayan, P. Jankowski, C. Njel, A. Roy, T. Vegge, J. Maibach, J. M. G. Lastra, M. Fichtner, Z. Zhao-Karger, *Angew. Chem., Int. Ed.* **2020**, *59*, 11483.

[69] E. Levi, M. D. Levi, O. Chasid, D. Aurbach, *J. Electroceram.* **2009**, *22*, 13.

[70] E. Levi, E. Lancry, A. Mitelman, D. Aurbach, G. Ceder, D. Morgan, O. Isnard, *Chem. Mater.* **2006**, *18*, 5492.

[71] J. Richard, A. Benayad, J. F. Colin, S. Martinet, *J. Phys. Chem. C* **2017**, *121*, 17096.

[72] C. Ling, K. Suto, *Chem. Mater.* **2017**, *29*, 3731.

[73] A. Mitelman, E. Levi, E. Lancry, D. Aurbach, *ECS Trans.* **2007**, *3*, 109.

[74] R. Zhang, F. Mizuno, C. Ling, *Chem. Commun.* **2015**, *51*, 1108.

[75] J. Niu, Z. Zhang, D. Aurbach, *Adv. Energy Mater.* **2020**, *10*, 2000697.

[76] K. Taniguchi, T. Yoshino, Y. Gu, Y. Katsura, H. Takagi, *J. Electrochem. Soc.* **2014**, *162*, A198.

[77] E. Levi, Y. Gofer, D. Aurbach, *Chem. Mater.* **2010**, *22*, 860.

[78] Z. Xue, D. He, X. Xie, *J. Mater. Chem. A* **2015**, *3*, 19218.

[79] M. Mao, Y. Tong, Q. Zhang, Y.-S. Hu, H. Li, X. Huang, L. Chen, L. Gu, L. Suo, *Nano Lett.* **2020**, *20*, 6852.

[80] J. Rouxel, *Chem. - Eur. J.* **1996**, *2*, 1053.

[81] Y. Wang, Z. Liu, C. Wang, X. Yi, R. Chen, L. Ma, Y. Hu, G. Zhu, T. Chen, Z. Tie, J. Ma, J. Liu, Z. Jin, *Adv. Mater.* **2018**, *30*, 1802563.

[82] K. Taniguchi, Y. Gu, Y. Katsura, T. Yoshino, H. Takagi, *Appl. Phys. Express* **2015**, *9*, 011801.

[83] M. Mao, C. Yang, Z. Lin, Y. Tong, Q. Zhang, L. Gu, L. Hong, L. Suo, Y.-S. Hu, H. Li, X. Huang, L. Chen, *JACS Au* **2021**, *1*, 1266.

[84] S. Dey, J. Lee, S. Britto, J. M. Stratford, E. N. Keyzer, M. T. Dunstan, G. Cibin, S. J. Cassidy, M. Elgaml, C. P. Grey, *J. Am. Chem. Soc.* **2020**, *142*, 19588.

[85] Z. Li, X. Mu, Z. Zhao-Karger, T. Diemant, R. J. Behm, C. Kübel, M. Fichtner, *Nat. Commun.* **2018**, *9*, 5115.

[86] K. W. Nam, S. Kim, S. Lee, M. Salama, I. Shterenberg, Y. Gofer, J.-S. Kim, E. Yang, C. S. Park, J.-S. Kim, S.-S. Lee, W.-S. Chang, S.-G. Doo, Y. N. Jo, Y. Jung, D. Aurbach, J. W. Choi, *Nano Lett.* **2015**, *15*, 4071.

[87] B. Pan, J. Huang, N. Sa, S. M. Brombosz, J. T. Vaughey, L. Zhang, A. K. Burrell, Z. Zhang, C. Liao, *J. Electrochem. Soc.* **2016**, *163*, A1672.

[88] M. Salama, I. Shterenberg, L. J. W. Shimon, K. Keinan-Adamsky, M. Afri, Y. Gofer, D. Aurbach, *J. Phys. Chem. C* **2017**, *121*, 24909.

[89] P. Canepa, S. Jayaraman, L. Cheng, N. N. Rajput, W. D. Richards, G. S. Gautam, L. A. Curtiss, K. A. Persson, G. Ceder, *Energy Environ. Sci.* **2015**, *8*, 3718.

[90] L. F. Wan, B. R. Perdue, C. A. Apblett, D. Prendergast, *Chem. Mater.* **2015**, *27*, 5932.

[91] H. Dong, Y. Liang, O. Tutusaus, R. Mohtadi, Y. Zhang, F. Hao, Y. Yao, *Joule* **2019**, *3*, 782.

[92] X. Xue, R. Chen, C. Yan, P. Zhao, Y. Hu, W. Kong, H. Lin, L. Wang, Z. Jin, *Adv. Energy Mater.* **2019**, *9*, 1900145.

[93] P. Novák, J. Desilvestro, *J. Electrochem. Soc.* **1993**, *140*, 140.

[94] F. Wang, X. Fan, T. Gao, W. Sun, Z. Ma, C. Yang, F. Han, K. Xu, C. Wang, *ACS Cent. Sci.* **2017**, *3*, 1121.

[95] R. Verrelli, A. P. Black, C. Pattanathummasid, D. S. Tchitchekova, A. Ponrouch, J. Oró-Solé, C. Frontera, F. Bardé, P. Rozier, M. R. Palacín, *J. Power Sources* **2018**, *407*, 162.

[96] I. D. Johnson, B. J. Ingram, J. Cabana, *ACS Energy Lett.* **2021**, *6*, 1892.

[97] N. Sa, H. Wang, D. L. Proffit, A. L. Lipson, B. Key, M. Liu, Z. Feng, T. T. Fister, Y. Ren, C.-J. Sun, J. T. Vaughey, P. A. Fenter, K. A. Persson, A. K. Burrell, *J. Power Sources* **2016**, *323*, 44.

[98] Y. Xu, X. Deng, Q. Li, G. Zhang, F. Xiong, S. Tan, Q. Wei, J. Lu, J. Li, Q. An, L. Mai, *Chem* **2019**, *5*, 1194.

[99] Z. Zhao-Karger, M. E. G. Bardaji, O. Fuhr, M. Fichtner, *J. Mater. Chem. A* **2017**, *5*, 10815.

[100] D.-M. Kim, S. C. Jung, S. Ha, Y. Kim, Y. Park, J. H. Ryu, Y.-K. Han, K. T. Lee, *Chem. Mater.* **2018**, *30*, 3199.

[101] M. Okoshi, Y. Yamada, A. Yamada, H. Nakai, *J. Electrochem. Soc.* **2013**, *160*, A2160.

[102] J. Shi, J. Zhang, J. Guo, J. Lu, *Nanoscale Horiz.* **2020**, *5*, 1467.

[103] R. Attias, M. S. Chae, B. Dlugatch, M. Oliel, Y. Goffer, D. Aurbach, *ACS Catal.* **2020**, *10*, 7773.

[104] O. Tutusaus, R. Mohtadi, T. S. Arthur, F. Mizuno, E. G. Nelson, Y. V. Sevryugina, *Angew. Chem., Int. Ed.* **2015**, *54*, 7900.

[105] Z. Li, T. Diemant, Z. Meng, Y. Xiu, A. Reupert, L. Wang, M. Fichtner, Z. Zhao-Karger, *ACS Appl. Mater. Interfaces* **2021**, *13*, 33123.

[106] P. Saha, P. H. Jampani, M. K. Datta, C. U. Okoli, A. Manivannan, P. N. Kumta, *J. Electrochem. Soc.* **2014**, *161*, A593.

[107] L. E. Blanc, X. Sun, A. Shyamsunder, V. Duffort, L. F. Nazar, *Small Methods* **2020**, *4*, 2000029.

[108] L. Hu, J. R. Jokisaari, B. J. Kwon, L. Yin, S. Kim, H. Park, S. H. Lapidus, R. F. Klie, B. Key, P. Zapol, B. J. Ingram, J. T. Vaughey, J. Cabana, *ACS Energy Lett.* **2020**, *5*, 2721.

[109] S. Grugeon, S. Laruelle, R. Herrera-Urbina, L. Dupont, P. Poizot, J. M. Tarascon, *J. Electrochem. Soc.* **2001**, *148*, A285.

[110] N.-W. Li, Y.-X. Yin, S. Xin, J.-Y. Li, Y.-G. Guo, *Small Methods* **2017**, *1*, 1700094.

[111] R. Attias, M. Salama, B. Hirsch, R. Pant, Y. Gofer, D. Aurbach, *ACS Energy Lett.* **2019**, *4*, 209.

[112] R. Mohtadi, M. Matsui, T. S. Arthur, S.-J. Hwang, *Angew. Chem., Int. Ed.* **2012**, *51*, 9780.

[113] T. Chen, G. Ceder, G. S. Gautam, P. Canepa, *Front. Chem.* **2019**, *7*, 24.

[114] D. Wang, X. Du, G. Chen, F. Song, J. Du, J. Zhao, Y. Ma, J. Wang, A. Du, Z. Cui, X. Zhou, G. Cui, *Angew. Chem., Int. Ed.* **2023**, *135*, e202217709.

[115] B. Li, R. Masse, C. Liu, Y. Hu, W. Li, G. Zhang, G. Cao, *Energy Storage Mater.* **2019**, *22*, 96.

[116] J. G. Connell, M. Zorko, G. Agarwal, M. Yang, C. Liao, R. S. Assary, D. Strmcnik, N. M. Markovic, *ACS Appl. Mater. Interfaces* **2020**, *12*, 36137.

[117] J. Drews, P. Jankowski, J. Häcker, T. Li, T. Danner, J. M. G. Lastra, T. Vegge, N. Wagner, K. A. Friedrich, Z. Zhao-Karger, M. Fichtner, A. Latz, *ChemSusChem* **2021**, *14*, 4820.

[118] A. Mukherjee, S. Taragin, H. Aviv, I. Perelshtein, M. Noked, *Adv. Funct. Mater.* **2020**, *30*, 2003518.

[119] W. Zhao, Z. Pan, Y. Zhang, Y. Liu, H. Dou, Y. Shi, Z. Zuo, B. Zhang, J. Chen, X. Zhao, X. Yang, *Angew. Chem., Int. Ed.* **2022**, *61*, e202205187.

[120] H. S. Kim, T. S. Arthur, G. D. Allred, J. Zajicek, J. G. Newman, A. E. Rodnyansky, A. G. Oliver, W. C. Boggess, J. Muldoon, *Nat. Commun.* **2011**, *2*, 427.

[121] J. Bitenc, K. Pirnat, T. Bančič, M. Gaberšček, B. Genorio, A. Randon-Vitanova, R. Dominko, *ChemSusChem* **2015**, *8*, 4128.

[122] S. Yagi, T. Ichitsubo, Y. Shirai, S. Yanai, T. Doi, K. Murase, E. Matsubara, *J. Mater. Chem. A* **2014**, *2*, 1144.

[123] T. Gao, X. Ji, S. Hou, X. Fan, X. Li, C. Yang, F. Han, F. Wang, J. Jiang, K. Xu, C. Wang, *Adv. Mater.* **2018**, *30*, 1704313.

[124] A. Du, Z. Zhang, H. Qu, Z. Cui, L. Qiao, L. Wang, J. Chai, T. Lu, S. Dong, T. Dong, H. Xu, X. Zhou, G. Cui, *Energy Environ. Sci.* **2017**, *10*, 2616.

[125] J. Häcker, C. Danner, B. Sievert, I. Biswas, Z. Zhao-Karger, N. Wagner, K. A. Friedrich, *Electrochim. Acta* **2020**, *338*, 135787.

[126] D. Muthuraj, A. Ghosh, A. Kumar, S. Mitra, *ChemElectroChem* **2019**, *6*, 684.

[127] M. Salama, R. Attias, B. Hirsch, R. Yemini, Y. Gofer, M. Noked, D. Aurbach, *ACS Appl. Mater. Interfaces* **2018**.

[128] T. Gao, M. Noked, A. J. Pearse, E. Gillette, X. Fan, Y. Zhu, C. Luo, L. Suo, M. A. Schroeder, K. Xu, S. B. Lee, G. W. Rubloff, C. Wang, *J. Am. Chem. Soc.* **2015**, *137*, 12388.

[129] Z. Zhao-Karger, X. Zhao, D. Wang, T. Diemant, R. J. Behm, M. Fichtner, *Adv. Energy Mater.* **2015**, *5*, 1401155.

[130] S.-Y. Ha, Y.-W. Lee, S. W. Woo, B. Koo, J.-S. Kim, J. Cho, K. T. Lee, N.-S. Choi, *ACS Appl. Mater. Interfaces* **2014**, *6*, 4063.

[131] B. P. Vinayan, Z. Zhao-Karger, T. Diemant, V. S. K. Chakravadhanula, N. I. Schwarzburger, M. A. Cambaz, R. J. Behm, C. Kubel, M. Fichtner, *Nanoscale* **2016**, *8*, 3296.

[132] W. Li, S. Cheng, J. Wang, Y. Qiu, Z. Zheng, H. Lin, S. Nanda, Q. Ma, Y. Xu, F. Ye, M. Liu, L. Zhou, Y. Zhang, *Angew. Chem.* **2016**, *128*, 6516.

[133] A. Robba, A. Vizintin, J. Bitenc, G. Mali, I. Arcon, M. Zitnik, K. Bucar, G. Aquilanti, C. Martineau-Corcos, A. Randon-Vitanova, R. Dominko, *Chem. Mater.* **2017**, *29*, 9555.

[134] B. P. Vinayan, H. Euchner, Z. Zhao-Karger, M. A. Cambaz, Z. Li, T. Diemant, R. J. Behm, A. Gross, M. Fichtner, *J. Mater. Chem. A* **2019**, *7*, 25490.

[135] R. Richter, J. Häcker, Z. Zhao-Karger, T. Danner, N. Wagner, M. Fichtner, K. A. Friedrich, A. Latz, *ACS Appl. Energy Mater.* **2020**, *3*, 8457.

[136] R. Richter, J. Häcker, Z. Zhao-Karger, T. Danner, N. Wagner, M. Fichtner, K. A. Friedrich, A. Latz, *ACS Appl. Energy Mater.* **2021**, *4*, 2365.

[137] Y. Nakayama, R. Matsumoto, K. Kumagae, D. Mori, Y. Mizuno, S. Hosoi, K. Kamiguchi, N. Koshitani, Y. Inaba, Y. Kudo, H. Kawasaki, E. C. Miller, J. N. Weker, M. F. Toney, *Chem. Mater.* **2018**, *30*, 6318.

[138] G. Mali, *Acta Crystallogr. C* **2017**, *73*, 229.

[139] T. Chen, G. S. Gautam, P. Canepa, *Chem. Mater.* **2019**, *31*, 8087.

[140] J. Häcker, D. H. Nguyen, T. Rommel, Z. Zhao-Karger, N. Wagner, K. A. Friedrich, *ACS Energy Lett.* **2022**, *7*, 1.

[141] T. Gao, S. Hou, F. Wang, Z. Ma, X. Li, K. Xu, C. Wang, *Angew. Chem., Int. Ed.* **2017**, *56*, 13526.

[142] G. Bieker, J. Wellmann, M. Kolek, K. Jalkanen, M. Winter, P. Bieker, *Phys. Chem. Chem. Phys.* **2017**, *19*, 11152.

[143] V. Duffort, X. Sun, L. F. Nazar, *Chem. Commun.* **2016**, *52*, 12458.

[144] Q. Zou, Y. Sun, Z. Liang, W. Wang, Y. C. Lu, *Adv. Energy Mater.* **2021**, *11*.

[145] A. Du, Y. Zhao, Z. Zhang, S. Dong, Z. Cui, K. Tang, C. Lu, P. Han, X. Zhou, G. Cui, *Energy Storage Mater.* **2020**, *26*, 23.

[146] Z. Zhao-Karger, X.-M. Lin, C. B. Minella, D. Wang, T. Diemant, R. J. Behm, M. Fichtner, *J. Power Sources* **2016**, *323*, 213.

[147] S.-B. Son, T. Gao, S. P. Harvey, K. X. Steirer, A. Stokes, A. Norman, C. Wang, A. Cresce, K. Xu, C. Ban, *Nat. Chem.* **2018**, *10*, 532.

[148] X. Zhou, J. Tian, J. Hu, C. Li, *Adv. Mater.* **2018**, *30*, 1704166.

[149] J. Sun, C. Deng, Y. Bi, K.-H. Wu, S. Zhu, Z. Xie, C. Li, R. Amal, J. Luo, T. Liu, D.-W. Wang, *ACS Appl. Energy Mater.* **2020**, *3*, 2516.

[150] D. Huang, S. Tan, M. Li, D. Wang, C. Han, Q. An, L. Mai, *ACS Appl. Mater. Interfaces* **2020**, *12*, 17474.

**ADVANCED
SCIENCE NEWS**

www.advancedsciencenews.com

**ADVANCED
ENERGY
MATERIALS**

www.advenergymat.de

[151] Y. Xu, Y. Ye, S. Zhao, J. Feng, J. Li, H. Chen, A. Yang, F. Shi, L. Jia, Y. Wu, X. Yu, P.-A. Glans-Suzuki, Y. Cui, J. Guo, Y. Zhang, *Nano Lett.* **2019**, *19*, 2928.

[152] X. Yu, A. Manthiram, *ACS Energy Lett.* **2016**, *1*, 431.

[153] L. Wang, P. Jankowski, C. Njel, W. Bauer, Z. Li, Z. Meng, B. Dasari, T. Vegge, J. M. G. Lastra, Z. Zhao-Karger, M. Fichtner, *Adv. Sci.* **2022**, *9*, 2104605.

[154] L. Zeng, N. Wang, J. Yang, J. Wang, Y. NuLi, *J. Electrochem. Soc.* **2017**, *164*, A2504.

[155] W. Wang, H. Yuan, Y. NuLi, J. Zhou, J. Yang, J. Wang, *J. Phys. Chem. C* **2018**, *122*, 26764.

[156] S. Zhang, Y. Huang, Y. NuLi, B. Wang, J. Yang, J. Wang, *J. Phys. Chem. C* **2020**, *124*, 20712.

[157] Y. Huang, S. Zhang, Y. NuLi, B. Wang, J. Yang, J. Wang, *Chem. J. Chin. Univ.* **2021**, *42*, 794.

[158] P. He, H. O. Ford, L. C. Merrill, J. L. Schaefer, *ACS Appl. Energy Mater.* **2019**, *2*, 6800.

[159] B. Lee, J. Choi, S. Na, D.-J. Yoo, J. H. Kim, B. W. Cho, Y.-T. Kim, T. Yim, J. W. Choi, S. H. Oh, *Appl. Surf. Sci.* **2019**, *484*, 933.

[160] M. Wu, Y. Zhang, T. Li, Z. Chen, S.-a. Cao, F. Xu, *Nanoscale* **2018**, *10*, 12526.

[161] F. Xiong, Y. Fan, S. Tan, L. Zhou, Y. Xu, C. Pei, Q. An, L. Mai, *Nano Energy* **2018**, *47*, 210.

[162] M. Mao, T. Gao, S. Hou, F. Wang, J. Chen, Z. Wei, X. Fan, X. Ji, J. Ma, C. Wang, *Nano Lett.* **2019**, *19*, 6665.

[163] Z. Wang, S. Rafai, C. Qiao, J. Jia, Y. Zhu, X. Ma, C. Cao, *ACS Appl. Mater. Interfaces* **2019**, *11*, 7046.

[164] K. V. Kravchyk, R. Widmer, R. Erni, R. J.-C. Dubey, F. Krumeich, M. V. Kovalenko, M. I. Bodnarchuk, *Sci. Rep.* **2019**, *9*, 7988.

[165] Z. Zhang, B. Chen, H. Xu, Z. Cui, S. Dong, A. Du, J. Ma, Q. Wang, X. Zhou, G. Cui, *Adv. Funct. Mater.* **2018**, *28*, 1701718.

[166] M. Wu, Y. Zhang, H. Wu, A. Qin, X. Li, J. Shen, Z. Chen, S. a. Cao, T. Li, F. Xu, *Energy Technol.* **2019**, *7*, 1800777.

[167] S. Yang, F. Ji, Z. Wang, Y. Zhu, K. Hu, Y. Ouyang, R. Wang, X. Ma, C. Cao, *Electrochim. Acta* **2019**, *324*, 134864.

[168] X. Xue, R. Chen, X. Song, A. Tao, W. Yan, W. Kong, Z. Jin, *Adv. Funct. Mater.* **2021**, *31*, 2009394.

[169] D. Wu, W. Wang, Y. NuLi, J. Yang, J. Wang, *Electrochim. Acta* **2020**, *330*, 135354.

[170] Z. Li, S. Liu, B. P. Vinayan, Z. Zhao-Karger, T. Diemant, K. Wang, R. J. Behm, C. Kübel, R. Klingeler, M. Fichtner, *Energy Storage Mater.* **2019**, *21*, 115.

[171] F. Bertasi, F. Sepehr, G. Pagot, S. J. Paddison, V. Di Noto, *Adv. Funct. Mater.* **2016**, *26*, 4860.

[172] H. Tian, T. Gao, X. Li, X. Wang, C. Luo, X. Fan, C. Yang, L. Suo, Z. Ma, W. Han, C. Wang, *Nat. Commun.* **2017**, *8*, 14083.

[173] X. Li, T. Gao, F. Han, Z. Ma, X. Fan, S. Hou, N. Eidson, W. Li, C. Wang, *Adv. Energy Mater.* **2018**, *8*, 1701728.

[174] Y. NuLi, Z. Guo, H. Liu, J. Yang, *Electrochem. Commun.* **2007**, *9*, 1913.

[175] P. Wang, J. Kappler, B. Sievert, J. Häcker, K. Küster, U. Starke, F. Ziegler, M. R. Buchmeiser, *Electrochim. Acta* **2020**, *361*, 137024.

[176] P. Wang, K. Kuester, U. Starke, C. Liang, R. Niewa, M. R. Buchmeiser, *J. Power Sources* **2021**, *515*, 230604.

[177] P. Wang, J. Trück, J. Häcker, A. Schlosser, K. Küster, U. Starke, L. Reinders, M. R. Buchmeiser, *Energy Storage Mater.* **2022**, *49*, 509.

[178] P. Wang, J. Truck, S. Niesen, J. Kappler, K. Kuster, U. Starke, F. Ziegler, A. Hintennach, M. R. Buchmeiser, *Batteries Supercaps* **2020**, *3*, 1239.

[179] S. Zhang, W. Ren, Y. NuLi, B. Wang, J. Yang, J. Wang, *Chem. Eng. J.* **2022**, *427*, 130902.

[180] H. Yuan, Y. Yang, Y. NuLi, J. Yang, J. Wang, *J. Mater. Chem. A* **2018**, *6*, 17075.

[181] Z. Zhao-Karger, M. Fichtner, *Front. Chem.* **2019**, *6*, 656.

[182] B. T. McAllister, L. T. Kyne, T. B. Schon, D. S. Seferos, *Joule* **2019**, *3*, 620.

[183] N.-A. Tran, N. D. Van Thanh, M. L. P. Le, *Chem. - Eur. J.* **2021**, *27*, 9198.

[184] H. Sano, H. Senoh, M. Yao, H. Sakaebe, T. Kiyobayashi, *Chem. Lett.* **2012**, *41*, 1594.

[185] B. Pan, D. Zhou, J. Huang, L. Zhang, A. K. Burrell, J. T. Vaughey, Z. Zhang, C. Liao, *J. Electrochem. Soc.* **2016**, *163*, A580.

[186] Z. Song, Y. Qian, M. L. Gordin, D. Tang, T. Xu, M. Otani, H. Zhan, H. Zhou, D. Wang, *Angew. Chem., Int. Ed.* **2015**, *54*, 13947.

[187] B. Pan, J. Huang, Z. Feng, L. Zeng, M. He, L. Zhang, J. T. Vaughey, M. J. Bedzyk, P. Fenter, Z. Zhang, A. K. Burrell, C. Liao, *Adv. Energy Mater.* **2016**, *6*, 1600140.

[188] Y. Xiu, Z. Li, V. B. Parambath, Z. Ding, L. Wang, A. Reupert, M. Fichtner, Z. Zhao-Karger, *Batteries Supercaps* **2021**, *4*, 1850.

[189] Z. Zhao-Karger, R. Liu, W. Dai, Z. Li, T. Diemant, B. P. Vinayan, C. B. Minella, X. Yu, A. Manthiram, R. J. Behm, M. Ruben, M. Fichtner, *ACS Energy Lett.* **2018**, *3*, 2005.

[190] A. B. Ikhe, J. Y. Seo, W. B. Park, J.-W. Lee, K.-S. Sohn, M. Pyo, *J. Power Sources* **2021**, *506*, 230261.

[191] Y. Xiu, A. Mauri, S. Dinda, Y. Pramudya, Z. Ding, T. Diemant, A. Sarkar, L. Wang, Z. Li, W. Wenzel, M. Fichtner, Z. Zhao-Karger, *Angew. Chem., Int. Ed.* **2023**, *62*, e202212339.

[192] Y. Zhang, J. Xie, Y. Han, C. Li, *Adv. Funct. Mater.* **2015**, *25*, 7300.

[193] H. Li, T. Ichitsubo, S. Yagi, E. Matsubara, *J. Mater. Chem. A* **2017**, *5*, 3534.

[194] Z. Zhang, H. Xu, Z. Cui, P. Hu, J. Chai, H. Du, J. He, J. Zhang, X. Zhou, P. Han, G. Cui, L. Chen, *J. Mater. Chem. A* **2016**, *4*, 2277.

[195] B. Pan, Z. Feng, N. Sa, S.-D. Han, Q. Ma, P. Fenter, J. T. Vaughey, Z. Zhang, C. Liao, *Chem. Commun.* **2016**, *52*, 9961.

[196] H. Dong, Y. Li, Y. Liang, G. Li, C.-J. Sun, Y. Ren, Y. Lu, Y. Yao, *Chem. Commun.* **2016**, *52*, 8263.

[197] Y. Li, Q. An, Y. Cheng, Y. Liang, Y. Ren, C.-J. Sun, H. Dong, Z. Tang, G. Li, Y. Yao, *Nano Energy* **2017**, *34*, 188.

[198] R. Zhang, O. Tutusaus, R. Mohtadi, C. Ling, *Front. Chem.* **2018**, *6*, 611.

[199] W. Li, E. M. Erickson, A. Manthiram, *Nat. Energy* **2020**, *5*, 26.

[200] T. Ichitsubo, S. Okamoto, T. Kawaguchi, Y. Kumagai, F. Oba, S. Yagi, N. Goto, T. Doi, E. Matsubara, *J. Mater. Chem. A* **2015**, *3*, 10188.

[201] H. Li, N. L. Okamoto, T. Hatakeyama, Y. Kumagai, F. Oba, T. Ichitsubo, *Adv. Energy Mater.* **2018**, *8*, 1801475.

[202] C. Li, W. Wu, Y. Liu, X. Yang, Z. Qin, X. Jia, X. Sun, *J. Power Sources* **2022**, *520*, 230853.

[203] X. Bian, Y. Gao, Q. Fu, S. Indris, Y. Ju, Y. Meng, F. Du, N. Bramnik, H. Ehrenberg, Y. Wei, *J. Mater. Chem. A* **2017**, *5*, 600.

[204] H. Du, Z. Zhang, J. He, Z. Cui, J. Chai, J. Ma, Z. Yang, C. Huang, G. Cui, *Small* **2017**, *13*, 1702277.

[205] Y. Yang, W. Wang, Y. Nuli, J. Yang, J. Wang, *ACS Appl. Mater. Interfaces* **2019**, *11*, 9062.

[206] Y. Li, P. Zuo, N. Zhang, X. Yin, R. Li, M. He, H. Huo, Y. Ma, C. Du, Y. Gao, G. Yin, *Chem. Eng. J.* **2021**, *403*, 126398.

[207] K. Tang, A. Du, S. Dong, Z. Cui, X. Liu, C. Lu, J. Zhao, X. Zhou, G. Cui, *Adv. Mater.* **2020**, *32*, 1904987.

[208] R. D. Rauh, K. M. Abraham, G. F. Pearson, J. K. Surprenant, S. B. Brummer, *J. Electrochem. Soc.* **1979**, *126*, 523.

[209] M. Wang, X. Li, M. Gao, H. Pan, Y. Liu, *J. Alloys Compd.* **2014**, *603*, 158.

[210] H. Fan, Z. Zheng, L. Zhao, W. Li, J. Wang, M. Dai, Y. Zhao, J. Xiao, G. Wang, X. Ding, H. Xiao, J. Li, Y. Wu, Y. Zhang, *Adv. Funct. Mater.* **2020**, *30*, 1909370.

[211] C. Wang, Y. Huang, Y. Lu, H. Pan, B. B. Xu, W. Sun, M. Yan, Y. Jiang, *Nano-Micro Lett.* **2021**, *13*, 195.

[212] B. Ouyang, J. Wang, T. He, C. J. Bartel, H. Huo, Y. Wang, V. Lacivita, H. Kim, G. Ceder, *Nat. Commun.* **2021**, *12*, 5752.

[213] J. Wang, S. Tan, G. Zhang, Y. Jiang, Y. Yin, F. Xiong, Q. Li, D. Huang, Q. Zhang, L. Gu, Q. An, L. Mai, *Sci. China Mater.* **2020**, *63*, 1651.

Zhenyou Li is currently an associate professor at Qingdao Institute of Bioenergy and Bioprocess Technology (QIBEBT), Chinese Academy of Sciences. He received Ph.D. in materials science from the University of Chinese Academy of Sciences in 2016, during which he worked as a visiting scholar at Heidelberg University for 2 years. From 2017 to 2023, he was a research scientist at Helmholtz Institute Ulm and Karlsruhe Institute of Technology. Recently, he joined QIBEBT and initiated a research group working on multivalent batteries.

Joachim Häcker is a material scientist working in the battery research group of Dr. Maryam Nojabaee at the Institute of Engineering Thermodynamics (TT) at the German Aerospace Center (DLR) in Stuttgart. He studied material science at the University of Stuttgart and subsequently did his Ph.D. in the field of magnesium–sulfur batteries. Since 2016 he is involved in the research of metal–sulfur batteries, specifically focusing on the implementation of magnesium and calcium metal anodes.

Maximilian Fichtner is professor for solid state chemistry at the Ulm University and head of the department "Energy Storage Systems" at the Institute of Nanotechnology (INT) of the Karlsruhe Institute of Technology (KIT). He is the director of the Helmholtz-Institute Ulm for Electrochemical Energy Storage (HIU), scientific director of CELEST (Center for Electrochemical Energy Storage Ulm-Karlsruhe), and spokesperson of the German Cluster of Excellence "Energy Storage Beyond Lithium" (POLiS). He is also a member of the core team of a large scale, long-term European research initiative "BATTERY2030+" for battery research in Europe.

Zhirong Zhao-Karger is a research group leader for advanced battery materials at the Institute of Nanotechnology (INT) of the Karlsruhe Institute of Technology (KIT). She received her Ph.D. in organic chemistry at the University Hannover, Germany. After the postdoctoral research at the Catalysis Research Laboratory of the University of Heidelberg, she joined the INT as a research scientist in 2008 and has been working in the field of electrochemical energy storage for more than 10 years with a focus on post-lithium batteries, such as magnesium- and calcium-based systems.